SIGNAL DETECTION FOR HIGH-DENSITY MAGNETIC RECORDING SYSTEMS

YANG HONGMING

NATIONAL UNIVERSITY OF SINGAPORE

2005

SIGNAL DETECTION FOR HIGH-DENSITY MAGNETIC RECORDING SYSTEMS

YANG HONGMING

(B. Eng. & M. Eng., TSINGHUA UNIVERSITY, BEIJING, P.R.CHINA)

A THESIS SUBMITTED

FOR THE DEGREE OF MASTER OF ENGINEERING

DEPARTMENT OF ELECTRICAL & COMPUTER ENGINEERING

NATIONAL UNIVERSITY OF SINGAPORE

2005

Acknowledgments

I would like to express my most sincere gratitude to my supervisor, Dr. George Mathew, who has led me into the exciting area of signal processing for magnetic recording systems, and worked with me closely throughout the past two years. Without his invaluable guidance, I could not have finished my study at National University of Singapore. But what I learn from him is much more than how to do research and present our work, his positive attitude towards his work has even changed the way I view my life. I can hardly expect any more from a supervisor, and I will try to be such a devoted person to my work in my future career.

I would also like to thank Ashwin Kumar, He An and Fabian Lim. I would not have such a good time at NUS without their great help.

I am also indebted to all the staff and students in Data Storage Institute, especially Dr. Guo Guoxiao, Ms. Cai Kui, Dr. Lin Yu, Dr. Chan Kheong Sann, Huang Li, Zou Xiaoxin, Peh Chester and Nurulhuda Binte Ibrahim who have helped me in quite a lot of different ways.

Finally, I would like to thank my parents for their solid support.

Contents

Summary

Motivated by the increasing demand for storage density and high-speed data retrieval in magnetic recording systems, efforts are underway investigating detection approaches that have optimum or close-to-optimum performances with low computational complexity and high detection speed. In this thesis, we study generalized partial response target design and post-processing approaches for signal detection in high-density magnetic recording channels with jitter noise. We also investigate the performance of sliding block Viterbi detector in the context of high-speed detection.

We consider high-density perpendicular magnetic recording channels with jitter noise and propose a novel approach to jointly design optimum generalized partial response (PR) target and linear equalizer. A new cost function, which accounts for the data-dependent nature of jitter noise, is developed based on minimum mean square error criterion. Using the step response based channel model, we derive expressions for the statistics required to compute the optimum equalizer and target in the presence of jitter noise. We present an approach for doing simulations as well as analytical computations for the jitter noise channel, without resorting to the widely used Taylor series approximations. We present computational and

simulation results to show that the targets designed by our approach give significant bit error rate (BER) performance improvement over the targets designed without accounting for the jitter under high jitter conditions. When the targets designed by our approach are used, there is no sign of error-floor effect for the range of signal to noise ratios (SNRs) considered.

To further enhance the signal detection performance for perpendicular channels with jitter noise, we propose a novel two-step post-processing approach for signal detection. The first step is to identify all the possible error regions from the normal Viterbi detector (VD) output using a simple threshold-based approach, and the second step is to re-detect only these regions using approaches that exploit the data-dependent characteristics of jitter noise. Thus, the resulting complexity increase is mostly limited to the short length of post-processing regions. Computational and simulation results show that the post-processing approach can reduce the complexity of the complicated sequence detection approaches greatly with minor performance loss or even performance enhancement at certain SNRs.

We also analyze the performance of sliding block Viterbi detector (SBVDet) for the purpose of designing its key parameters. A detailed algorithm to obtain characteristics of all the catastrophic and non-catastrophic error events for a VD without knowing the starting/ending states of its input sequence is presented. Through the error event analysis and simulation results, we show that SBVDet can increase the speed of VD without limit and with almost no influence on the BER performance and error event distribution. An intuitive approach to do error event analysis for simpler PR targets is also presented.

List of Symbols and Abbreviations

a_n	input data bit
b_n	transition data
g_k	coefficients of target response
$h(t)$	pulse/dibit response of recording channel
$h_s(t)$	step response of recording channel
$h_{tr}(t)$	transition response of recording channel
$p(\cdot)$	probability density function
w_k	coefficients of linear equalizer
$x\|y$	x conditioned on y
$E[\cdot]$	expectation operator
$G(z)$	Z-transform of target response
$\mathbf{P}$	cross-correlation matrix
$Pr(X)$	probability of X
$Q(\alpha)$	probability of zero-mean unit variance Gaussian tail $[\alpha, \infty]$

$\mathbf{R}$	autocorrelation matrix
T	duration of one channel bit
$W(z)$	Z-transform of equalizer response
Δ_m	transition position jitter
ACSU	add-compare-select unit
AWGN	additive white Gaussian noise
BCJR	Bahl, Cocke, Jelinek, Raviv
BER	bit error rate
BM	branch metric
DFE	decision feedback equalization
ECC	error control coding
GPR	generalized partial response
ISI	inter-symbol interference
MAP	maximum *a posteriori*
ML	maximum likelihood
MLSD	maximum-likelihood sequence detector
MMSE	minimum mean square error
NRZI	non-return to zero inverse
PM	path metric
PR	partial response
PRML	partial response maximum likelihood

SBVD	sliding block Viterbi decoder
SBVDet	sliding block Viterbi detector
SNR	signal to noise ratio
VA	Viterbi algorithm
VD	Viterbi detector
VD-MV	Viterbi detector with mean and variance compensation for noise
VD-NP	Viterbi detector with noise prediction
ZF	zero-forcing

List of Figures

List of Tables

Chapter 1

Introduction

In this chapter, we present a brief overview of magnetic recording system. After introducing perpendicular magnetic recording, we will focus on the signal processing techniques used in recording channels. Thereafter, the motivation and summary of the research work in this thesis are presented. Finally, the organization of the thesis is given.

1.1 Magnetic Recording Systems

The advent of the information technology has created a tremendous demand for mass data storage and high-speed retrieval of digital data. Further, the demand for storage capacity and signal retrieval speed has been increasing all the time, as a result of the development of various applications of information technology and the increasing need to store, transmit and play high-quality multimedia contents.

To serve this need, magnetic recording has played an important role and continuously undergone substantial advancements throughout its history. Magnetic hard disks have become necessary and irreplaceable components of computers and var-

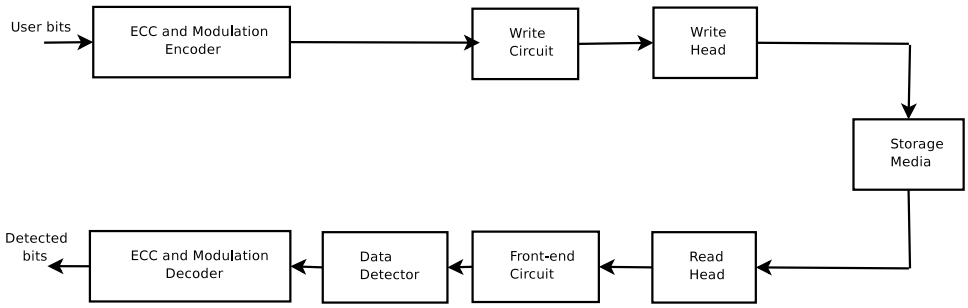

Figure 1.1: Block diagram of a digital magnetic recording system.

ious daily applications. The development of current digital media players, such as IPod, *etc.*, also provides vivid examples of the importance of magnetic recording to the information age as well as people's daily lives.

Over the past five decades, breakthroughs in head and media technology have been the major contributing factors to the spectacular growth in storage capacity. However, signal processing and coding techniques have also been playing an important role in providing cost-efficient means to enhance the storage capacity [31]. Hence the research on signal processing for magnetic recording has always been a promising field.

A block schematic of a magnetic recording system is shown in Figure 1.1. The user information bits are first fed to an ECC (error control coding) encoder, which incorporates error detection and correction capabilities into the user bits. After that, a modulation encoder matches the user data to the recording channel characteristics, thus reducing the channel distortion effects to improve detection performance, and to ensure proper working of control loops (*e.g.* timing/gain recovery) at the receiver. Following the ECC/modulation encoder, the write circuit converts the coded data into write current using NRZI (non-return to zero inverse) modulation technique [31]. The write head then magnetizes the storage medium to saturation in directions according to the polarity of the write current waveform. In the readback process, the read head generates voltage output signal, which is induced by the magnetic flux associated with the transitions in the magnetization

pattern on the medium. The front-end circuit in general consists of a low-pass filter to limit the noise bandwidth, a sampler to generate discrete signals, timing recovery and gain control circuits, and an equalizer to shape the overall channel response so that the signal detector is able to recover the stored data reliably. The data detector recovers the encoded data and passes them to an ECC and modulation decoder, which recovers the original user information bits.

The signal path from the input of write circuit to output of read head is called the magnetic recording channel. Since the readback voltage signal reflects transitions in the data pattern stored on the medium, under reasonable conditions, the magnetic recording channel can be modeled by transition response and the readback signal can be modeled as linear superposition of transition responses. It is obvious that the channel response to an isolated bit at the input is linearly related to transition response, and thus we can also model the magnetic recording channel using bit response. From the above, we may say that the magnetic recording channel resembles a base-band digital communication system with pulse amplitude modulation (PAM).

The signal read from the magnetic recording channel is corrupted by inter-symbol interference (ISI), various electronics/media noises, and some non-linear distortions. In general, all these distortions will increase with increase in recording density. The purpose of signal processing therefore is to minimize the channel distortions and recover the information bits as reliably as possible.

Analog peak detection can be used in low-density magnetic recording, but it cannot provide satisfactory performance when the ISI is high, which is the normal condition for high-density magnetic recording. Thus, partial response maximum-likelihood (PRML) detection was introduced in early 1990s [11], which significantly raised the storage density capability.

Extensive research work has been done for longitudinal recording [31]. However,

the perpendicular magnetic recording has better potential for supporting high-density magnetic recording [21, 22] and the channel characteristics are different from those of longitudinal recording, and hence the signal processing strategies need to be re-investigated for perpendicular magnetic recording. Furthermore, at high densities, the media noise, which is non-linear, data-dependent and colored, becomes the dominant channel distortion rather than electronics noise which can be viewed as additive white Gaussian noise (AWGN). Thus, special signal processing techniques have to be used to take care of the non-linear, data-dependent and colored media noise. In this thesis, we relocate the media noise problem using an accurate channel model and focus on optimum joint equalizer-target design to account for media noise.

Several applications require detection algorithms with low-complexity and high-speed. To increase the signal detection reliability for high-density magnetic recording, we have to use more complex signal processing techniques, which will result in high-complexity implementations and speed bottleneck. The high-complexity requirement and speed bottleneck will constraint the applications of advanced signal processing techniques. Thus, in this thesis, we also look into the implementation issues and focus on low-complexity and high-speed detection algorithms.

1.2 Perpendicular Magnetic Recording

In magnetic recording systems, areal recording density can be increased by reducing all physical dimensions proportionally, including bit length, head size, and the thickness of granular medium, *etc.*, as well as refining the medium micro-structure, in particular, reducing the size of ferromagnetic grains in the media.

But in current longitudinal recording systems, reducing the bits and grain sizes may cause the so-called "super paramagnetic effect" [54], thereby limiting the

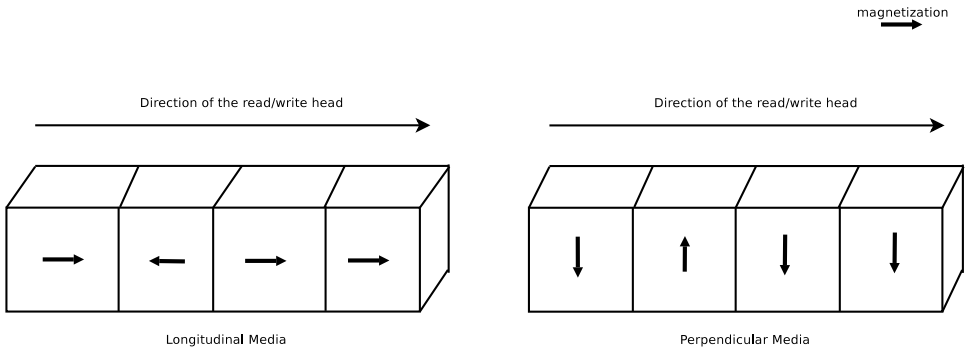

Figure 1.2: Magnetization pattern of storage medium for longitudinal and perpendicular magnetic recording.

achievable areal density. However, perpendicular recording technique is expected to provide much greater potential for supporting high-density magnetic recording [22]. As shown in Figure 1.2, in the perpendicular recording, the magnetization direction on the storage medium is perpendicular to the direction of write/read head. It is expected to replace the longitudinal recording technology in a few years.

Current longitudinal recording system may achieve storage density as high as 100 gigabits per square inch (Gb/inch^2) [48]. On the other hand, using perpendicular recording technology, Hitachi Global Storage Technologies has demonstrated an areal density of 230 (Gb/in2) [1], which is the highest areal density achieved to date based on vertical recording. Clearly it represents a doubling of today's highest data densities based on longitudinal recording technology.

Besides the promising ultra-high densities and many other advantages [55], perpendicular recording also bring more challenges to the medium, read/write heads and signal processing techniques. In other words, advanced signal processing techniques are also needed to combat the problems arising in perpendicular magnetic recording systems.

1.3 Characteristics of Channel Distortions in Magnetic Recording

In order to use signal processing techniques to achieve high recording density with reliable data retrieval, we need to investigate the characteristics of channel distortions in magnetic recording. The major distortions in recording channels are linear ISI, noises (electronics and media noises), non-linear distortions, *etc.*

1.3.1 Linear ISI

Interference corresponds to the presence of signals other than those intended in the readback signal. In magnetic recording channels, the isolated transition/bit response spans more than one bit interval, which leads to overlapping of transition/bit responses due to adjacent transitions/bits. The resulting interference from adjacent symbols, other than the one in the current position, is called ISI.

At higher densities, the transition/bit responses become much "wider" with respect to a bit interval, and thus result in severe ISI. Equivalently in frequency domain, if we observe the bandwidth of the channel, we can see that the normalized channel bandwidth with respect to bit rate becomes smaller at higher densities, which also represents increasing ISI.

Full response or partial response equalization is normally used to reduce ISI. Nonetheless, practical equalizers always result in some residual ISI. The residual ISI influences the detector performance seriously especially when we use Viterbi-like maximum likelihood detectors, which we will explain later. Thus, when we design equalizers and target responses, we always want to minimize residual ISI as much as possible.

1.3.2 Noise

Channel noise originates in the medium, the head, the head preamplifier, *etc.* As a rule, none of these distortions is negligible. Different noise sources can be viewed as mutually independent.

Head noise and thermal noise in preamplifier, which are sources of electronics noise, can be modeled as additive white Gaussian noise (AWGN). On the other hand, media noise, which arises due to irregularities and imperfections of the medium, turns out to be correlated, non-stationary and data-dependent. It can be modeled by the microtrack model, the signal-dependent autoregressive channel model and the position jitter and width variation model [24, 37].

Media noise is negligible at low recording densities, whereas it becomes the dominant noise source at high recording densities. Consequently, the equalization and detection techniques that are developed for channels with significant AWGN (compared to media noise) cannot be used for data retrieval in high-density systems. Hence, special signal processing techniques need to be used to take care of media noise in high-density magnetic recording.

1.3.3 Non-linear distortions

Non-linear distortions refer to the phenomena that violate the linear superposition principle in magnetic recording channels. As density increases, closely spaced magnetic transitions start to interact, which results in severe non-linear effects, such as non-linear transition shift (NLTS), transition broadening, partial erasure, and overwriting, *etc* [29]. It is obvious that the non-linear effects will also become severe at high recording densities. To minimize the non-linearities, we can use modulation codes such as maximum transition run (MTR) codes to limit consecutive transitions and write pre-compensation techniques [6].

In summary, almost all distortions become severe at high densities, thus requiring more advanced signal processing techniques. Since non-linear distortions can be effectively controlled during writing process, we will focus on the receiver design for recording channels corrupted by linear ISI, electronics noise and media noise.

1.4 Survey of Existing Work

In this section, we present a brief review of detection techniques for high-density magnetic recording. The review first focuses on typical PRML schemes which is developed without considering media noise. Thereafter, optimum detection schemes and generalized PR targets design approaches to combat media noise are summarized. Finally, we provide a survey of high-speed Viterbi detection.

1.4.1 PRML Detection Techniques

Sequence detector is preferable than symbol-by-symbol threshold detector in magnetic recording, in spite of higher complexity and decision delay, because it can provide much better performance to combat the serious ISI in magnetic recording.

Most of the widely used sequence detectors are based on the principle of maximum-likelihood sequence detector (MLSD), which is simpler to implement than maximum-a-posteriori sequence detector (MAP-SD). Further, MLSD and MAP-SD are equivalent if each possible transmitted sequence is equally probable. When the channel noise is AWGN, MLSD can be efficiently implemented using the Viterbi Algorithm (VA). Note that even when the channel noise is not perfectly AWGN, VA is still preferable because of its high computational efficiency in spite of small performance loss.

In magnetic recording, the Viterbi Detector (VD) is always preceded by a linear partial response (PR) equalizer, which shapes the channel response into a shorter predefined target response to help VD and reduce the complexity. Hence it is called partial response maximum-likelihood (PRML) detector[1].

The performance of VD will degrade significantly if the noise level is very high or the noise samples are highly correlated at VD input. Hence, the design problem in PRML is to reduce the noise level as well as noise correlation at the input of VD. This problem can be resolved partially through the design of equalizers and PR target responses.

The equalizer is meant to match the channel response to some predefined target response. It can be categorized into zero-forcing (ZF) and minimum mean square error (MMSE) equalizers [3]. The ZF equalizer has the inherent disadvantage of noise enhancement and this problem becomes severe in high-density magnetic recording. Hence, MMSE equalizer is more preferable in high-density recording systems.

As to the design of target response, standard PR targets with integer coefficients are normally employed, which are chosen by simple inspection of their match to the channel response. The widely used PR targets for longitudinal recording are PR Class 4 (PR4) $(1 - D^2)$, extended PR4 (EPR4) $(1 + D - D^2 - D^3)$, *etc.* in the standard form of $(1 - D)(1 + D)^n$, where D denotes 1-bit delay operator and n is a positive number [49]. For perpendicular recording, the widely used standard PR targets are those with only positive coefficients such as $1 + 2D + D^2$, $1 + 2D + 2D^2 + D^3$, $1 + 2D + 3D^2 + 2D^3 + D^4$, *etc* [41]. Although PRML systems based on standard PR targets are easy to implement, the performance degrades significantly at high recording densities. The reason is these relatively short targets

[1]Traditionally, in recording systems, the receiver consisting of a PR equalizer followed by VD is called PRML, even though this receiver is not optimum in the sense of ML since the noise at VD input is not white.

do not match the channel response very well, resulting in severe residual ISI, and hence limiting the detection performance of VD. Moreover, these targets do not effectively account for the presence of media noise in the channel.

The generalized PR (GPR) targets with real-valued coefficients can match the channel response more closely and provide better detector performance. Clearly, this gain is achieved at the cost of increase in complexity, since the real-valued target coefficients necessitate multiplication of real-numbers as compared to integer-valued target coefficients. With the development of very large scale integration (VLSI) systems, this increase in complexity seems to be a minor problem. Hence extensive research has been focused on design of GPR targets. The widely used method is to jointly design target response and PR equalizer based on MMSE criterion [35]. To avoid trivial all-zero solutions, some constraint needs to be imposed on the target, such as monic-constraint, which requires the first tap of the target to be one, fixed-energy constraint, which requires the energy in the target response to be one, *etc.* Among these constraints, the monic-constraint outperforms others because it can minimize the noise correlation at the VD input. This is because the forward equalizer in optimum decision feedback equalization (DFE) system can be viewed as a GPR system with some GPR target satisfying the monic-constraint that ensures that the noise samples at the detector input is close to AWGN.

Another approach developed to design GPR targets is based on dominant error events in the VD [9,35]. That is, the target is designed by minimizing the probabilities of the dominant error events at VD output. However, this is a chicken-and-egg approach to the problem, since changing the target response will change the dominant error events. Nevertheless, it has not been found to outperform the MMSE approach significantly.

1.4.2 Optimum Detection and GPR Targets Design to Combat Media Noise

The review in Section 1.4.1 does not consider media noise. However, at high recording densities, the detection performance of PRML detectors suffer seriously due to media noise, which is the dominant disturbance in high-density magnetic recording channels. Unlike the most commonly used noise model of additive white Gaussian and data-independent electronics noise, as mentioned already, the media noise is correlated, data-dependent, non-stationary and non-additive in nature [47].

Several approaches have been proposed in the literature to deal with the problem of degradation in detection performance due to media noise. One sort of approach is through designing optimum detectors. Moon and Park [34] proposed a pattern-dependent noise-predictive maximum-likelihood detector. By modeling the media noise as a finite-order Markov process [24], Kavčić and Moura [23] developed an optimum sequence detector using optimized branch metrics. Chen and Trachtenberg [10] proposed an approach that asymptotically becomes ML. Since optimum detectors usually result in high computational complexity, there have been several proposals for sub-optimum approaches that are simpler to implement. For example, modifications in the branch metrics of the VD were proposed by Zeng and Moon [58] to account for the data-dependent variance of media noise and by Sun *et al.* [46] to account for the data-dependent mean of media noise.

Another sort of approach to deal with media noise is through designing GPR target to minimize the noise correlation since the noise should be white Gaussian for VD to be optimum. This approach helps to improve the detector performance significantly compared to standard PR targets with integer coefficients. Caroselli *et al.* [7] was the first to employ data-dependent noise prediction for media noise channels. Moon and Zeng [35] studied the effect of different constraints in the design of GPR targets for channels with jitter noise. They reported the supe-

riority of monic constraint (*i.e.* first tap of the target is set to 1) in dealing with noise correlation and getting performance close to that of the optimum target designed by maximizing the so-called "effective SNR" of VD. Oenning and Moon [37] presented an analytical solution for monic-constrained GPR targets for Lorentzian model based channels with media noise. An adaptive approach for designing monic-constrained GPR targets with data-dependent adaptation for compensating nonlinearities caused by medium and head, was proposed by Zayed and Carley [57]. Whereas all the references quoted above deal with longitudinal recording, Sawaguchi *et al.* [45] and Kovintavewat *et al.* [25] presented target design approaches for perpendicular recording channels with jitter noise. While they also use the monic constraint, the targets of Sawaguchi *et al.* [45] incorporate DC-suppression of varying degrees in view of the low-frequency disturbances (*e.g.* jitter noise, thermal asperity, *etc.*) in practical channels. Okamoto *et al.* [39] extended the data-dependent noise prediction approach to perpendicular recording to deal with jitter noise. The performance of several standard PR targets (with integer-valued coefficients) for perpendicular channels with jitter noise was studied by Okamoto *et al.* [41].

1.4.3 High-Speed Viterbi Detection

The Viterbi algorithm was first presented as a means to decode convolutional codes [52], and was later proven to be an efficient algorithm for maximum-likelihood sequence detection in channels with ISI [19]. Implementation of the Viterbi detector (VD) mainly comprises three parts: a branch metric computation unit (BMU), an add-compare-select unit (ACSU), and a survivor memory unit (SMU). The BMU and SMU can be easily implemented using pipelined structures, while the ACSU has a data-dependent non-linear feedback loop, which makes the ACSU to be the bottleneck in high-speed implementations of VD [15].

Various methods have been introduced to break the ACSU-bottleneck. One

approach is to transform the structure of ACSU to reduce the length of the critical path, such as M-step/1-step algorithm, carry-save algorithm, latch-based parallel ACS method, and a double-state architecture [4, 13, 15–18, 26, 50]; but there still exists a speed limit decided by the new critical path. The other approach, which is presented in [5, 14, 28], uses block-wise parallel implementation to boost the speed. The "minimized method Viterbi decoding" approach presented in [14] can increase the speed infinitely, but, each received sample is processed twice by the VD, and hence the computational complexity is about twice of conventional VD. The "zero-shift" method presented in [28] requires the information source to insert K zeros after each block, where K is the memory length of the channel/target/code. Hence this method results in performance loss due to loss in information rate, unless the block length is sufficiently large. Further, the "reset method" used in [28] to avoid the loss in information rate resets the memory content of the Markov source before transmitting a new subblock. But it may lead to performance loss due to the insufficient truncation length of the trellis and result in different (and undesirable) error event distribution compared to conventional VD. The sliding block Viterbi decoder (SBVD) of Black and Meng [5] results in unlimited concurrency and hence high throughput due to independent block decoding. A look-up table implementation of the sliding block decoding approach was earlier proposed by Tzou and Dunham [51]. The SBVD approach does not impose any constraint on the encoding process in comparison to the approach of Lin and Messerschmitt [28]. Moreover, it is truly a maximum likelihood (ML) decoding algorithm, and hence its performance upper bounds that of the "minimized method" of Fettweis *et al.* [14]. Therefore, in this thesis, we focus on the application of sliding block approach for signal detection on PR equalized magnetic recording channels, which is called sliding block Viterbi detector (SBVDet) in this thesis.

1.5 Motivation and Summary of the Present Work

In this thesis, we focus on signal processing techniques for high-density magnetic recording channels with jitter noise and high-speed implementations of VD. Our motivation lies in the need for low-complexity and high-speed detection approaches that have close-to-optimum performances. We design optimum GPR target and equalizer for perpendicular recording channels with jitter noise, based on MMSE criterion. We also propose a two-step post-processing approach to improve the performance of traditional VD approach with minor increase of computational complexity. We also present an analysis of the performance of SBVDet for magnetic recording channels for the purpose of designing its key parameters.

1.5.1 Joint Design of Optimum PR Target and Equalizer for Recording Channels with Jitter Noise

The most commonly used approach for modeling media noise is by incorporating position-jitter and width-variation in the step response. However, to minimize the effort required in simulating the readback signal as well as to facilitate analytically feasible approaches for designing equalizer and target, it has been a common practice to approximate the step response containing position-jitter and width-variation by using the Taylor series expansion with terms up to first or second order [10, 34, 37]. This approximation turns out to be quite inaccurate at high recording densities and/or with large jitter and width-variation. On the other hand, without making these approximations, the problem of target design has never been addressed for media noise channels in the literature. Furthermore, the simulation of the media noise channel is itself a very tedious task without these approximations.

Therefore, in this thesis, we re-investigate the GPR target design problem without approximating the channel model. We introduce a new mean square error (MSE) based cost function considering media noise, electronics noise, and ISI for jointly designing the equalizer and target. This cost function accounts for the data-dependent nature of media noise. We also derive expressions for computing the statistics required for evaluating the coefficients of the optimum GPR target and linear equalizer. Computational and simulation results are presented to show that while the targets designed without accounting for the jitter lead to error-floor in the bit error rate performance, the targets designed by our approach give significant performance improvement under high jitter conditions, with no sign of error-floor effect for the range of SNRs considered.

1.5.2 A Novel Post-Processing Approach for Signal Detection in Channels with Jitter Noise

The GPR targets and equalizers designed by us are shown to be able to reduce the effect of transition jitter effectively. However, we observe that the BER performance is still much worse than the case without transition jitter in the channel. This means that the media noise is still a major disturbance in the channel, and it motivates us to investigate further approaches to combat media noise combined with the GPR targets and equalizers designed above.

We look into signal detection approaches that account for the data-dependency of media noise. As mentioned in Section 1.4.2, there are some optimum detection approaches to combat media noise. However, the computational complexity of these approaches is much higher than that of normal VD, and is the main obstacle in using these approaches in practical hard drive systems. Hence, we aim to develop new approaches that have close-to-optimum performances with moderate increase in complexity.

To improve the BER performances of detectors while avoiding the complexity increase, we propose a novel two-step post-processing approach in this thesis. The first step is to identify all the possible error regions from the normal VD output using a simple threshold-based approach, and the second step is to re-detect only these regions using approaches that can tackle the data-dependent characteristics of jitter noise. Thus, the complexity increase is mostly limited to the post-processing regions, which are quite short in length.

Computational and simulation results show that the post-processing approach can reduce the complexity of the complicated sequence detection approaches with minor performance loss or even performance enhancement at different SNRs.

1.5.3 Analysis and Design of Sliding Block Viterbi Detector for Magnetic Recording Channels

As introduced in Section 1.4.3, the SBVDet approach is quite an advantageous approach to enhance the detection speed. Therefore, we focus on performance analysis and key parameter design of SBVDet approach for magnetic recording channels.

Since the SBVDet is a block-wise detection approach, we present a detailed algorithm to obtain characteristics of all the catastrophic and non-catastrophic error events for a VD without knowing the starting/ending states of a sequence. Through the error event analysis and simulation results, we show that SBVDet can increase the speed of VD without limit and with almost no influence on the BER performance and error event distribution. We also present an intuitive approach to do error event analysis for simpler PR targets.

1.6 Organization of the Thesis

Chapter 2 presents a detailed overview of signal processing techniques for magnetic recording. Joint design of optimum generalized partial response target and equalizer for perpendicular recording channels with jitter noise is addressed in Chapter 3. In Chapter 4, we present a novel post-processing approach for signal detection in high-density magnetic recording channels with transition jitter. Chapter 5 presents analysis of the performance and the design of key parameters of sliding block Viterbi detector (SBVDet) for magnetic recording channels. Finally in Chapter 6, we conclude the work reported in this thesis and present some possible directions of future work.

Chapter 2

Background on Signal Processing for Magnetic Recording

In this chapter, we present an overview of widely used channel models for digital magnetic recording with and without considering media noise. Based on the channel models, we focus on the signal processing techniques used in the receiver design, namely, equalization and signal detection to counter-act the channel distortions in magnetic recording channels. As introduced in Chapter 1, PRML approach is preferable for magnetic recording, and hence we focus on the partial response (PR) equalization. After that, we review the various optimum and sub-optimum signal detection algorithms.

2.1 Discrete-Time Channel Model

In this section, we introduce the widely used approach to model the magnetic recording channel and some discrete-time channel models with and without considering media noise.

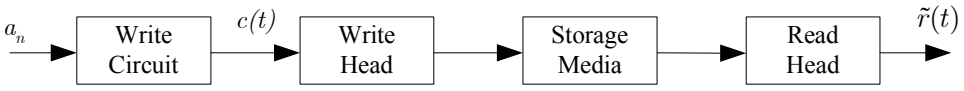

Figure 2.1: Block diagram of magnetic write/read processes.

2.1.1 Channel with Electronics Noise

We start modeling the magnetic recording system with electronics noise only, which is usually considered as AWGN.

Part of the schematic of the magnetic recording system from Figure 1.1 is redrawn in Figure 2.1. The objective of channel modeling is to obtain a mathematical expression relating the data bits a_n to the readback signal $\tilde{r}(t)$. The write circuit converts the coded data $a_n \in \{+1, -1\}$ into the write current $c(t)$. In this process, the write circuit can be viewed as a linear pulse modulator, and its impulse response is an ideal rectangular pulse with duration T and amplitude 1.0, given by

$$\tilde{p}(t) = \begin{cases} 1 & \text{for } 0 \leq t \leq T \\ 0 & \text{otherwise} \end{cases} \tag{2.1}$$

where T is the bit interval. Hence, the write current waveform $c(t)$ is a rectangular pulse sequence with amplitude equal to 1.0 or -1.0, corresponding to the bit sequence a_n. The $c(t)$ drives the write head to magnetize the material on the storage media to saturation in one of the two directions corresponding to the polarity of $c(t)$. The read head performs flux-to-voltage conversion, which generates a voltage signal $\tilde{r}(t)$ according to the directions of transitions in the magnetization on the media, or equivalently, according to the transitions in the sequence a_n. For the transition from -1 to $+1$ (*i.e.*, a positive transition), the read head generates the waveform $2h_s(t)$, where $h_s(t)$ is the step response of the channel. For the transition from $+1$ to -1 in a_n (*i.e.* a negative transition), the read head generates a waveform $-2h_s(t)$. When there is no transition in a_n, the read head generates nothing.

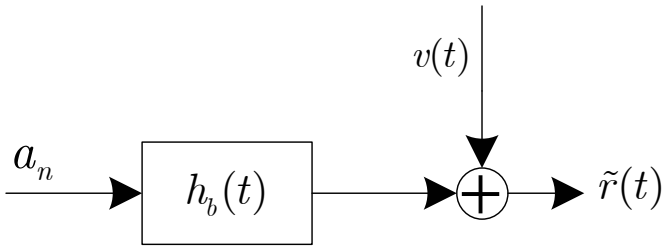

Figure 2.2: Continuous-time model for magnetic recording channel.

Thus, we may model the magnetic recording channel using the step response $h_s(t)$ as

$$\tilde{r}(t) = \sum_n (a_n - a_{n-1}) h_s(t - nT) + \tilde{v}(t) \tag{2.2}$$

where $\tilde{v}(t)$ is the electronics noise, which is AWGN. Equivalently, we may define the bit response of the channel as $h_b(t) = h_s(t) - h_s(t - T)$ and model the channel as

$$\tilde{r}(t) = \sum_n a_n h_b(t - nT) + \tilde{v}(t) \tag{2.3}$$

as depicted in Figure 2.2. Note that we can also define a transition response of the channel as

$$h_{tr}(t) = 2h_s(t). \tag{2.4}$$

Sufficient statistics for recovering the data bits a_n from analog readback signal $\tilde{r}(t)$ can be obtained by passing $\tilde{r}(t)$ through a matched filter with impulse response $h_b(-t)$ and a symbol-rate sampler to sample the matched-filter output at rate $1/T$ samples/sec [19]. But in practice, accurate channel response $h_b(t)$ might not be known, and hence a low-pass filter (LPF) is usually used in place of the matched filter.

Since the data rate is $1/T$, the desired bandwidth is also $1/T$. If the bandwidth of the channel $h_b(t)$ exceeds $1/T$, over-sampling with a sampler rate $1/T_s$ (*i.e.* $T_s < T$) is used instead of $1/T$ to ensure that the detection performance is insensitive to the sampling phase [20]. Here T_s is chosen such that the bandwidth of $h_b(t)$

is less than $1/T_s$. Therefore, the equalizer that follows the sampler should be a fractionally-spaced equalizer (FSE) with tap-spacing $T_s < T$. For high-density magnetic recording, the bandwidth of $h_b(t)$ is usually less than $1/T$, and hence over-sampling and the associated FSE are not necessary. Since our focus in this thesis is high-density recording, we shall henceforth use a T-spaced system model. Since the channel is strictly band-limited to $(-\frac{1}{2T}, \frac{1}{2T})$, the front-end consisting of an ideal low-pass filter in the band $(-\frac{1}{2T}, \frac{1}{2T})$ and a bit-rate sampler can also provide a set of sufficient statistics for recovering the data bits a_n.

After passing $\tilde{r}(t)$ through an ideal low-pass filter of bandwidth $1/T$ and a T-spaced sampler, the resulting discrete-time signal $r(mT)$ can be written as

$$r(mT) = \sum_n a_n h_b(mT - nT) + v(mT) \tag{2.5}$$

where $r(t)$ and $v(t)$ are the low-pass filter outputs corresponding to $\tilde{r}(t)$ and $\tilde{v}(t)$, respectively, and mT denotes the m^{th} sampling instant, with m being an integer. Let r_m, h_m and v_m denote $r(mT)$, $h_b(mT)$ and $v(mT)$, respectively. Thus, we obtain the discrete-channel model as

$$r_m = \sum_n a_n h_{m-n} + v_m \tag{2.6}$$

as depicted in Figure 2.3. Since $\tilde{v}(t)$ is white, the power spectral density of the filtered noise $v(t)$ is also white in the band $(-\frac{1}{2T}, \frac{1}{2T})$. Consequently, the sampled noise v_m is a discrete-time white noise. The power of v_m is given by $\frac{N_0}{T}$ where $\frac{N_0}{2}$ is the power spectral density of $\tilde{v}(t)$. Further, v_m is also Gaussian since $\tilde{v}(t)$ is Gaussian.

Based on experimental data, the step response in longitudinal recording is well

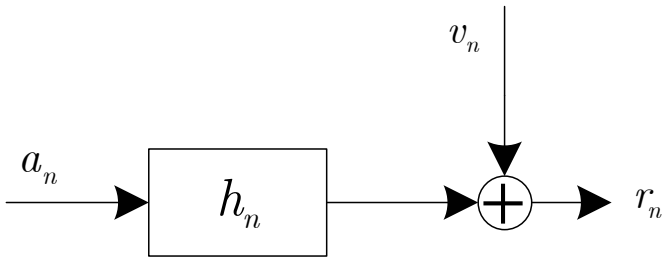

Figure 2.3: Discrete-time model for magnetic recording channel.

modeled by the Lorentzian pulse [33] given by

$$h_s(t) = \frac{V_p}{1 + \left(\frac{2t}{T_{50}}\right)^2} \tag{2.7}$$

where V_p is half of the base-to-peak amplitude of isolated transition response, and T_{50} is the temporal width of the pulse at its 50% amplitude level. T_{50} is also related to normalized linear density D_c by $T_{50} = D_c T$.

In perpendicular recording, the isolated step response is widely modeled either by an arctangent function [40] as

$$h_s(t) = \frac{V_p}{\pi} \arctan\left(\frac{2t}{T_{50}}\right) \tag{2.8}$$

or by a hyperbolic tangent function [45] as

$$h_s(t) = \frac{V_p}{2} \tanh\left(\frac{\ln 3}{T_{50}} t\right) \tag{2.9}$$

where T_{50} is the time required for $h_s(t)$ to rise from $-V_p/4$ to $V_p/4$. As before, we can define the normalized linear density as $D_c = T_{50}/T$. The channel signal-to-noise ratio (SNR) is defined as

$$\text{SNR} = 10 \log_{10}\left(\frac{V_{op}^2}{\sigma_v^2}\right) \tag{2.10}$$

where $V_{op} = 2V_p$ and σ_v^2 is the variance of v_n. In this thesis, we will be using the hyperbolic tangent function based perpendicular channel model.

In practice, we can truncate the sampled bit response of the recording channel, since the bit response tends to zero as t goes to $+\infty$ or $-\infty$. Thus the resulting channel model with electronics noise can be written as

$$r_n = \sum_{m=0}^{N_c-1} a_m h_{n-m} + v_n \tag{2.11}$$

where N_c is the effective length of the sampled bit response h_n after truncation.

2.1.2 Media Noise Model

As mentioned in Chapter 1, media noise becomes one of the dominant noise sources in high-density magnetic recording. Hence, it is important to model the media noise accurately in the development and study of detection techniques.

Widely used channel models incorporating media noise include the microtrack model [8], the signal-dependent autoregressive channel model [24] and the position jitter and width variation model [37]. The starting point for all these models is the fact that the main physical phenomenon responsible for media noise is the randomness associated with the shape of magnetization transitions on the medium [47]. Therefore, we shall focus on the position-jitter-width-variation model because that is more fundamental and closely related to the physical mechanisms responsible for generating media noise [30]. Because the position jitter effect is the major media noise effect and also for the sake of simplicity, we only consider position jitter effect in this thesis. Therefore, the channel model with media noise can be written as

$$r(nT) = \sum_m b_m h_s(nT - mT + \Delta_m) + v(nT) \tag{2.12}$$

where $\{b_m\}$ is the corresponding transition sequence (*i.e.*, $b_m = a_m - a_{m-1}$) with $b_m \in \{+2, 0, -2\}$, and Δ_m is the jitter in the transition at position m. The jitter sequence $\{\Delta_m\}$ is modeled as a sequence of independent Gaussian random variables which are truncated to the region $(-T/2, T/2)$.

For the sake of convenience in doing equalization and performing analysis, Taylor series based expansion is usually used to simplify the channel model (2.12). For example, first-order transition jitter model can be written as

$$r(nT) = \sum_m b_m h_s(nT - mT) + \sum_m b_m \Delta_m h_s^p(nT - mT) + v(nT) \tag{2.13}$$

where $h_s^p(nT - mT) = \frac{\partial h_s(t)}{\partial t}\|_{t=(n-m)T}$. Thus, (2.13) models the media noise as data-dependent additive noise. Based on this simplification, analysis of linear equalization and optimum detection have been done in [34, 37].

However, we know that the first-order approximation based simplified model (2.13) is acceptable only when the variance of transition jitter is small. But in high-density magnetic recording, the variance of transition jitter is actually quite large. Therefore, the first-order model (2.13) is quite inaccurate for high-density recording. In Chapter 3, we will look at the development of more accurate models.

2.2 Linear Partial Response Equalization

The purpose of equalization is to compensate for the distortions introduced by the channel on the data. We consider two channel distortions, namely, inter-symbol-interference (ISI) and channel noise, in this section.

The equalizer can be classified into full response and partial response (PR) equalizers [3]. Full response equalizer tries to remove all the ISI while PR equalizer tries to equalize the channel response into some predefined partial response. The

partial response allows some known ISI to remain over a short-span. In high-density magnetic recording, PR equalization based PRML system outperforms full response equalization based approach. This is because the high-density channels are quite band-limited in nature and hence full response equalization results in excessive noise enhancement.

Zero-forcing (ZF) and mean square error (MSE) are the two most widely used criteria for equalizer design [3]. The ZF approach tries to force the unwanted ISI to zero, but this may result in serious noise enhancement, especially in high-density magnetic recording. On the other hand, the MSE based approach tries to minimize the error at the equalizer output, and thus effectively reduce noise enhancement by allowing some residual ISI to remain at the equalizer output.

There is yet another kind of equalizer called decision-feedback equalizer (DFE), which is non-linear in nature [33]. The DFE based approach does not utilize the signal energy completely and has the added disadvantage of error-propagation. Hence, we will not discuss it further in this thesis.

In the following, we focus on PR equalization which is part of the PRML approach widely used in magnetic recording.

2.2.1 Zero-Forcing Partial Response Equalization

Figure 2.4 depicts the zero-forcing PR system model. Let $\{g_k\}$ denote the predefined PR target response with $G(z)$ being its z-transform. Similarly, let $\{w_k\}$ and $W(z)$ denote the impulse response and z-transform, respectively, of the equalizer. The z-transform of the channel bit response h_n is denoted by $H_b(z)$.

The ZF criterion requires the unwanted ISI to be zero, thus we get the optimum PR-ZF equalizer as

$$W_o(z) = \frac{G(z)}{H_b(z)}. \tag{2.14}$$

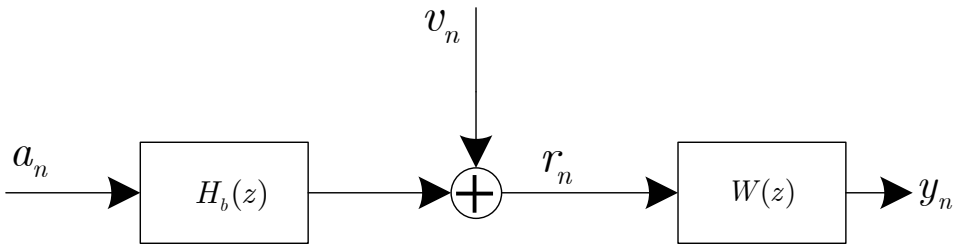

Figure 2.4: Schematic of zero-forcing partial response equalization. The equalizer $W(z)$ is chosen such that $H_b(z)W(z) = G(z)$, where $G(z)$ is the PR target.

The resulting equalizer output can be written as

$$y_n = \sum_k g_k a_{n-k} + \hat{v}_n \tag{2.15}$$

where $\hat{v}_n$ is the noise component at the equalizer output with power spectrum density (PSD) given by

$$\Phi_{\hat{v}\hat{v}}(e^{j\omega T}) = \frac{N_0}{2}|W_o(e^{j\omega T})|^2 = \frac{N_0}{2}\frac{|G(e^{j\omega T})|^2}{|H_b(e^{j\omega T})|^2} \tag{2.16}$$

with ω being the frequency in radians/sec.

We can see from (2.16) that the ZF-PR equalizer is in general an infinite impulse response (IIR) filter, and thus may have the problem of instability. Even if the filter is stable, the noise enhancement is inevitable for magnetic recording. Since the channel $\{h_k\}$ is infinitely long while the PR target $\{g_k\}$ is very short in length, it is almost impossible for $|G(e^{j\omega T})|$ to match $|H_b(e^{j\omega T})|$ at all the frequencies. The mis-match that happens in the frequency regions corresponding to close-to-zero values of $|H_b(e^{j\omega T})|$ causes severe noise enhancement. Even worse, when the channel response has intervals of zeros, the PR-ZF might not exist for finite-length PR target responses.

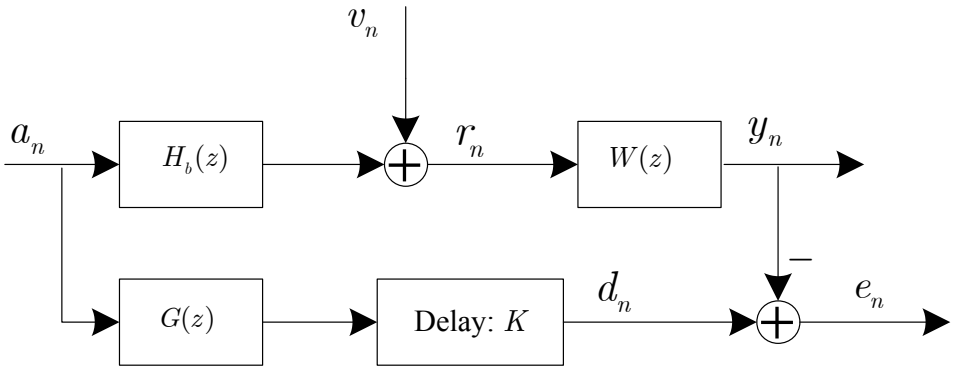

Figure 2.5: Schematic of MMSE partial response equalization.

2.2.2 Mean Square Error PR Equalization

To minimize the noise enhancement of ZF equalizers, we now consider equalizers based on MSE criterion. Figure 2.5 depicts the schematic illustrating MSE based PR equalization. The delay 'K' is meant to account for the delay from channel input to equalizer output. The equalizer is designed to minimize the mean square error between the desired output of the equalizer (*i.e.*, target output d_n) and the actual output y_n, and hence it is called minimum mean square error PR equalizer (MMSE-PR).

The error signal e_n is given by

$$\begin{aligned} e_n &= d_n - y_n \\ &= \sum_k g_k a_{n-K-k} - \sum_k (h \otimes w)_k a_{n-k} - \sum_l w_l v_{n-l} \end{aligned} \tag{2.17}$$

where '$\otimes$' denotes convolution. Note from Figure 2.5 that the PSD of y_n is given by[1]

$$\Phi_{yy}(e^{j\omega T}) = \Phi_{aa}|H_b|^2 + \Phi_{vv} \tag{2.18}$$

where $\Phi_{vv}(e^{j\omega T})$ and $\Phi_{aa}(e^{j\omega T})$ are the PSDs of v_n and a_n, respectively. Therefore,

[1]For the sake of convenience, we have left out the argument '$(e^{j\omega T})$' from the frequency-domain quantities $\Phi_{aa}(e^{j\omega T})$, $H_b(e^{j\omega T})$, $W(e^{j\omega T})$, $\Phi_{vv}(e^{j\omega T})$, $G(e^{j\omega T})$ and $\Phi_{yy}(e^{j\omega T})$ on the right side of (2.18) to (2.22).

with $\tilde{G}(e^{j\omega T}) = e^{-j\omega KT}G(e^{j\omega T})$, the PSD of e_n is given by

$$\begin{aligned}
\Phi_{ee}(e^{j\omega T}) &= \Phi_{aa}|H_bW - \tilde{G}|^2 + \Phi_{vv}|W|^2 \\
&= |G|^2\left[\Phi_{aa}\left|H_b\frac{W}{\tilde{G}} - 1\right|^2 + \Phi_{vv}\left|\frac{W}{\tilde{G}}\right|^2\right] \\
&= |G|^2\left[\Phi_{yy}\left|\frac{W}{\tilde{G}} - \Phi_{aa}\Phi_{yy}^{-1}H_b^*\right|^2 + \Phi_{aa}\Phi_{vv}\Phi_{yy}^{-1}\right] \qquad (2.19)
\end{aligned}$$

which result in the optimum equalizer to be

$$W_o(e^{j\omega T}) = \frac{\Phi_{aa}H_b^*\tilde{G}}{\Phi_{yy}} = \frac{\Phi_{aa}H_b^*Ge^{-j\omega KT}}{\Phi_{aa}|H_b|^2 + \Phi_{vv}}. \qquad (2.20)$$

where '$*$' denotes complex conjugation. Substituting (2.20) in (2.19), we obtain the optimum error PSD as

$$\Phi_{ee}(e^{j\omega T}) = \frac{\Phi_{aa}\Phi_{vv}|G|^2}{\Phi_{yy}} = \frac{\Phi_{aa}\Phi_{vv}|G|^2}{\Phi_{aa}|H_b|^2 + \Phi_{vv}}. \qquad (2.21)$$

From (2.21), we can see that target $G(e^{j\omega T})$ should be chosen such that

$$|G(e^{j\omega T})|^2 \propto \frac{\Phi_{aa}|H|^2 + \Phi_{vv}}{\Phi_{aa}\Phi_{vv}} \qquad (2.22)$$

to make the error e_n white, which means that there is no noise enhancement at all. But, this would require infinite-length target response. In other words, noise enhancement and error correlation cannot be avoided completely with finite-length target responses.

The above analysis is in frequency domain where we assumed infinite-length equalizer. But in practice, we can only have finite-length equalizers. Thus, it is important to show the results for finite-length equalization here.

Let N_g, N_w and N_h denote the lengths of target response, linear equalizer and

channel response, respectively, and

$$\begin{aligned} \mathbf{w} &= [w_0, w_1, \cdots, w_{N_w-1}]^T \\ \mathbf{y}_n &= [y_n, y_{n-1}, \cdots, y_{n-N_w+1}]^T \\ \mathbf{g} &= [g_0, g_1, \cdots, g_{N_g-1}]^T \\ \mathbf{a}_n &= [a_n, a_{n-1}, \cdots, a_{n-N_g+1}]^T. \end{aligned} \tag{2.23}$$

Then, we get

$$\begin{aligned} e_n &= d_n - y_n = \sum_{i=0}^{N_g-1} g_i a_{n-K-i} - \sum_{i=0}^{N_w-1} w_i y_{n-i} \\ &= \mathbf{g}^T \mathbf{a}_{n-K} - \mathbf{w}^T \mathbf{y}_n. \end{aligned} \tag{2.24}$$

Using this, we can get the MSE as

$$\begin{aligned} E[|e_n|^2] &= E[(d_n - \mathbf{w}^T \mathbf{y}_n)^2] \\ &= E[d_n^2] - \mathbf{p}^T \mathbf{w} - \mathbf{w}^T \mathbf{p} + \mathbf{w}^T \mathbf{R}_y \mathbf{w} \\ &= E[d_n^2] - 2\mathbf{w}^T \mathbf{p} + \mathbf{w}^T \mathbf{R}_y \mathbf{w} \end{aligned} \tag{2.25}$$

where $\mathbf{p} = E[\mathbf{y}_n d_n]$ and $\mathbf{R}_y = E[\mathbf{y}_n \mathbf{y}_n^T]$. Setting the gradient of $E[|e_n|^2]$ with respect to $\mathbf{w}$ to zero, we can obtain the optimum MMSE solution for finite-length PR equalizer as

$$\mathbf{w}_o = \mathbf{R}_y^{-1} \mathbf{p}. \tag{2.26}$$

In summary, MMSE-PR equalizer reduces ISI and noise enhancement at the same time. In general, it results in better performance than ZF-PR equalizer, especially at low SNRs. However, as we noted earlier, noise enhancement and error correlation can not be avoided completely for finite-length target responses.

On the other hand, optimality of Viterbi detector requires the error e_n to be white Gaussian. These remarks lead us to the following problem: How to design optimum finite-length PR target response and the associated finite-length equalizer to result in enhanced detection performance from Viterbi or Viterbi-like detectors? In response to this, we consider the design of target and equalizer in Chapter 3 and the modification of detection strategy in Chapter 4.

2.3 Optimum Signal Detection

In this section, we deal with optimum signal detection. The aim of detection is to recover the transmitted (or stored) data as reliably as possible. In channels with memory, it is natural that sequence detectors outperform symbol-by-symbol detectors. Hence, sequence detectors are widely used in magnetic recording. Therefore, we also focus on sequence detection in this thesis.

Let the vector $\mathbf{y}$ denote the received sequence of samples at the output of the linear equalizer, and let the vector $\hat{\mathbf{a}}$ denote the corresponding sequence of bit decisions at the detector output. The goal of a sequence detector is to find the detected bit sequence $\hat{\mathbf{a}}$ such that the probability of correct decision is maximized. Thus, the optimum detection criterion is the maximum-a-posteriori (MAP) criterion, which means that the detected sequence is the sequence such that the probability $\Pr(\hat{\mathbf{a}}|\mathbf{y})$ is maximized.

Using Bayes' rule, we can write

$$\Pr(\hat{\mathbf{a}}|\mathbf{y}) = \frac{p(\mathbf{y}|\hat{\mathbf{a}})}{p(\mathbf{y})} \tag{2.27}$$

where $p(\mathbf{y}|\hat{\mathbf{a}})$ is the likelihood function of receiving $\mathbf{y}$ when $\hat{\mathbf{a}}$ is transmitted. The detection of $\mathbf{a}$ based on maximization of the likelihood is called the maximum-

likelihood (ML) approach for optimum detection. It can be observed that ML detection is equivalent to MAP detection when all possible transmitted sequences are equally probable. In general, ML approach is simpler to implement, and hence it is more preferred in magnetic recording.

2.3.1 ML Sequence Detection and Viterbi Algorithm

The Viterbi algorithm (VA) is widely used for data detection in magnetic recording. When the error at equalizer output is assumed as AWGN, the VA is an efficient implementation of maximum likelihood sequence detection (MLSD). We give a short description of MLSD and VA in this section.

The output signal of linear equalizer can be expressed as[2] (see Figure 2.5)

$$y_n = \sum_{i=0}^{N_g-1} g_i a_{n-i} + e_n = d_n + e_n \tag{2.28}$$

with

$$d_n = a_n + \sum_{i=1}^{N_g} g_i a_{n-i} \tag{2.29}$$

where we assume $g_0 = 1$ without loss of generality.

The MLSD will give the output data vector according to

$$\hat{\mathbf{a}} = \arg\left\{\max_{\tilde{\mathbf{a}}} p(\mathbf{y}|\tilde{\mathbf{a}})\right\} \tag{2.30}$$

where $\tilde{\mathbf{a}}$ is one of the possible transmitted data sequence. For a sequence length N, MLSD computes the conditional joint probability density function (pdf) $p(\mathbf{y}|\mathbf{a})$ for each of the 2^N possible transmitted sequences and chooses the one that maximizes the joint pdf.

[2]For the sake of notational convenience, we suppress the delay K while writing y_n and d_n.

If we further assume the error signal e_n to be AWGN with its variance σ_e^2, we can write

$$\begin{aligned} p(\mathbf{y}|\tilde{\mathbf{a}}) &= \prod_{n=0}^{N-1} p(y_n|\tilde{\mathbf{a}}) \\ &= \prod_{n=0}^{N-1} \frac{1}{\sqrt{2\pi\sigma_e^2}} \exp\left(-\frac{|y_n - \tilde{d}_n|^2}{2\sigma_e^2}\right) \\ &= \left(\frac{1}{\sqrt{2\pi\sigma_e^2}}\right)^N \exp\left(-\frac{\sum_{n=0}^{N-1} |y_n - \tilde{d}_n|^2}{2\sigma_e^2}\right) \end{aligned}$$

where $\tilde{d}_n = \sum_{i=0}^{N_g-1} g_i \tilde{a}(n-i)$. Since σ_e^2 is a constant and exp(.) is a monotonic function, maximizing $p(\mathbf{y}|\tilde{\mathbf{a}})$ is equivalent to minimizing

$$J(\tilde{\mathbf{a}}) = \sum_{n=0}^{N-1} |y_n - \tilde{d}_n|^2 = ||\mathbf{y} - \tilde{\mathbf{d}}(\tilde{\mathbf{a}})||^2 \tag{2.31}$$

which is nothing but the Euclidean distance between the received vector $\mathbf{y}$ and the noiseless ideal equalizer output $\tilde{\mathbf{d}}(\tilde{\mathbf{a}})$ computed by assuming $\tilde{\mathbf{a}}$ as the transmitted data sequence.

Because the number of candidate sequences grows exponentially with N, the computational complexity required to implement the detector based on minimizing the Euclidean distance in (2.31) also grows exponentially. Therefore, it is almost impossible to implement the MLSD using (2.31), even though the detector based on (2.31) is already much simple compared to that based on (2.30).

The VA is an efficient algorithm for implementing the Euclidean distance minimization implied in (2.31). For the channel with finite memory, the noiseless output can be expressed using a finite-state representation. The principle of VA is to search for the optimum path through the trellis defined for this finite-state representation. Figure 2.6 depicts an example of the trellis for a channel with memory of 2 bits. A continuous line connecting two states represents an input bit

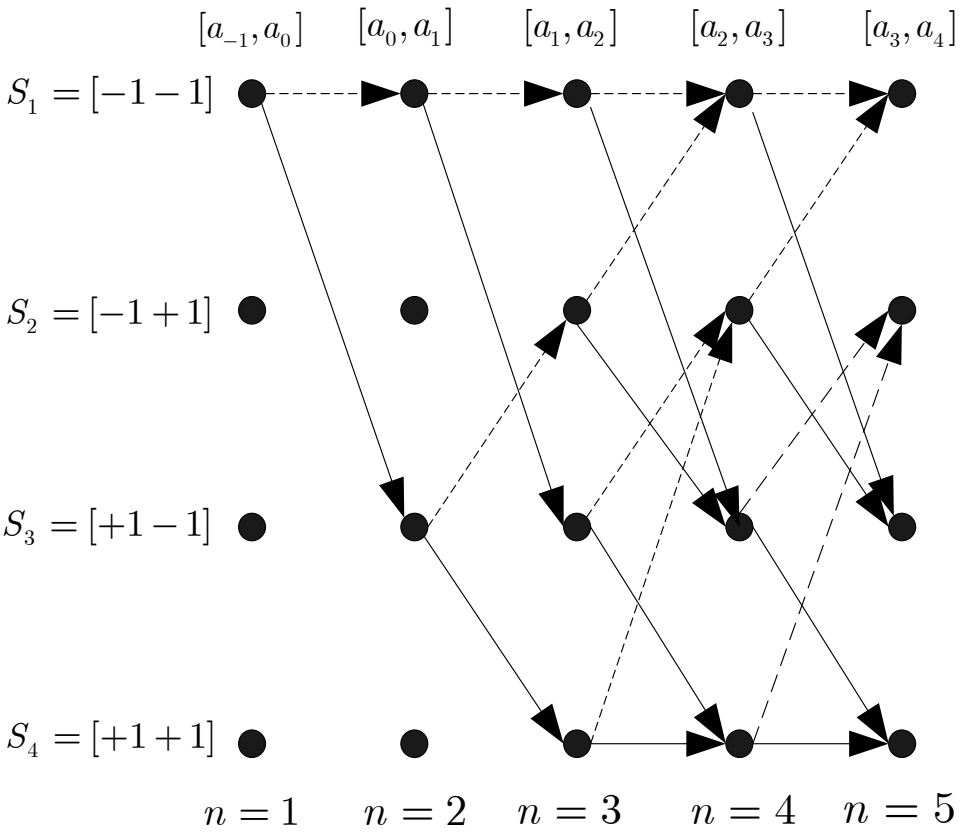

Figure 2.6: The trellis for a channel with memory of 2 bits. The states of the finite-state representation are given by S_1, S_2, S_3 and S_4, and the transition from one state to another represents the input data bit a_n associated with the path (or data sequence) that passes through this state transition.

to be $+1$ while a dotted line represents an input bit to be -1. Note that each possible transmitted data sequence has a corresponding unique path through the trellis.

Let $\mathbf{a}_k$ be the k^{th} path through the trellis. Then, define $J(\tilde{\mathbf{a}}_k)$ in (2.31) as the path metric (PM) associated with this path (or, the k^{th} candidate sequence) $\mathbf{a}_k$, and $BM_k(n) = |y_n - \tilde{d}_{k,n}|^2$ as the n^{th} branch metric (BM) associated with $\mathbf{a}_k$. Here, $d_{k,n}$ denotes the noiseless output of the equalizer at instant n corresponding to the candidate sequence $\mathbf{a}_k$. It is clear that the path metric of any candidate sequence is the sum of all the corresponding branch metrics. Since $PM_k(l) = \sum_{i=0}^{l} BM_k(i)$ is the path metric associated with candidate sequence $\mathbf{a}_k$ up until the l^{th} instant,

we can update the path metric as

$$PM_k(l) = PM_k(l-1) + BM_k(l). \tag{2.32}$$

As can be seen from Figure 2.6, each candidate sequence corresponds to one particular path through the trellis, and we can see that more than one path may arrive at any particular state at the same time. Assume that paths $\mathbf{a}_1$ and $\mathbf{a}_2$ pass through the same state S_i at instant m, and let $PM_1(m) > PM_2(m)$. Consider a path $\mathbf{b}$ from state S_i at instant m to the end of the sequence, and let the path metric associated with $\mathbf{b}$ be $PM_b = \sum_{i=(m+1)}^{N} BM_b(i)$. We can see that for any full sequence $\hat{\mathbf{a}}_1 = \{\mathbf{a}_1, \mathbf{b}\}$, there exists a sequence $\hat{\mathbf{a}}_2 = \{\mathbf{a}_2, \mathbf{b}\}$ such that $PM_{\hat{\mathbf{a}}_2}(m) < PM_{\hat{\mathbf{a}}_1}(m)$. This means that any path which has $\mathbf{a}_1$ in its beginning cannot be the optimum path, and hence all such paths can be eliminated from the search. Furthermore, this elimination of paths can be done at instant m instead of instant N. Thus, we can significantly simplify the search process. The path which results in the minimum partial path metric is called survivor path associated with the state S_i at instant m. During the searching process, we only need to save the survivor paths for each state, and finally get the overall optimum path at instant N.

It is clear that the path elimination process described above results in dropping half of the candidate sequences at each instant. This results in huge savings in computations and storage. In general, the computational complexity of VA increases linearly with N instead of being exponential. This is the advantage of VA compared to direct MLSD.

Finally, note that the VA is equivalent to optimum MLSD only when the channel noise is AWGN. Once this assumption is violated, the performance of VA will not be optimum or may be degraded badly. Thus, for the PRML system, the error

signal e_n at the input to the Viterbi detector (VD) is required to be as close to AWGN as possible. This requires a better PR target response and equalizer design so as to result in close-to-white error signal. Or, a noise-whitening filter can be inserted between the equalizer and the VD, resulting in the so-called noise-predictive maximum likelihood (NPML) sequence detector [12]. But NPML makes the effective channel response different from that defined by the original PR target, and hence the trellis structure of VD should be changed accordingly.

From the point of view of VD, it is easy to see why we would like to shape the channel response into a PR target with shorter length. Note that the number of states in the trellis increases exponentially with the increase of channel memory. Since the channel response of magnetic recording is usually very long, we need PR equalization to shorten the channel response so that VD can be employed with affordable complexity in hardware and computations.

2.4 Summary

In this chapter, we introduced the discrete-time channel model of digital magnetic recording channel with and without considering media noise. From the introduction, we can see that more accurate channel model without simplification such as the Taylor expansion needs to be used to handle the signal detection problem for high-density magnetic recording. Thereafter, we gave an overview of various signal processing techniques used in magnetic recording to recover the user bits reliably. We focused on the widely used PRML approach which comprises a partial response equalizer and Viterbi detector. Basic concepts related to PR equalizer and sequence detection were also presented.

Chapter 3

Joint Design of Optimum PR Target and Equalizer for Recording Channels with Jitter Noise

In this chapter, joint design of optimum generalized partial response (GPR) target and equalizer for perpendicular recording channels with jitter noise is addressed. We start with a discussion of a few different approaches for modeling high-density magnetic recording channels with media noise. Thereafter, we introduce a new cost function and derive an approach to compute optimum GPR target and equalizer based on minimum mean square error (MMSE) criterion. Computational and simulation results are also presented. We also present some additional comments, highlighting the distinctiveness of our work reported in this chapter. The work reported in this chapter has been accepted for publication in IEEE Trans. Magnetics [56].

3.1 Models for Channel with Media Noise

The magnetic recording channels are usually modeled by bit response $h_b(t)$ or step response $h_s(t)$, where $h_b(t) = h_s(t) - h_s(t-T)$ and T is the bit period. Since

the recording channel can be assumed to be band-limited at high densities, we use bit-rate sampled readback signal in this chapter. The resulting readback signal samples with only electronics noise can be written as

$$\begin{aligned} r_n &= \sum_m a_m h_b(nT - mT) + v_n \\ &= \sum_m b_m h_s(nT - mT) + v_n \end{aligned} \tag{3.1}$$

where $\{a_n\}$ is the recorded bit sequence with $a_n \in \{-1, +1\}$, $\{b_n\}$ is the corresponding transition sequence with $b_n = a_n - a_{n-1}$ and $b_n \in \{+2, 0, -2\}$, and v_n is white Gaussian electronics noise with variance σ_v^2.

Widely used channel models incorporating media noise include the microtrack model [8], the data-dependent autoregressive model [24], and the position jitter and width variation model [37]. We focus on the position jitter and width variation model in this chapter. Since position jitter effect is the major media noise effect [36], we only consider position jitter in this chapter. Thus, the readback signal with media noise can be written as

$$r_n = \sum_m b_m h_s(nT - mT + \Delta_m) + v_n \tag{3.2}$$

where Δ_m is the jitter in the position of transition corresponding to b_m and $\{\Delta_m\}$ are modeled as independent Gaussian random variables truncated to the range $(-T/2, T/2)$ with mean zero and variance σ_Δ^2. Clearly, $\Delta_m \neq 0$ only if $b_m \neq 0$.

It is easy to note from (3.2) that the presence of jitter causes the duration of the bits recorded on the medium to be different from T. For example, duration of the bit a_m on the medium is given by

$$T_m = T + \Delta_{m+1} - \Delta_m. \tag{3.3}$$

Using this information, we can express the readback signal in terms of the bit response as

$$r_n = \sum_m a_m h_{b,m}(nT - mT - \Delta_m) + v_n \tag{3.4}$$

where

$$h_{b,m}(t) = h_s(t) - h_s(t - T_m) \tag{3.5}$$

is the bit response corresponding to the bit a_m of duration T_m. The model (3.4) is as accurate as (3.2) itself since we did not use any approximations in deriving (3.4).

For the sake of convenience in generating the readback signal, designing equalizer and performing analysis, Taylor expansion is usually used to simplify the channel model (3.2). For example, first-order approximation of the channel model with transition jitter is given by

$$r_n \approx \sum_m b_m h_s(nT - mT) + \sum_m b_m \Delta_m h_i(nT - mT) + v_n \tag{3.6}$$

where $h_i(t) \triangleq \frac{\partial h_s(t)}{\partial t}$ is the impulse response of the channel. Thus the media noise gets modeled as an additive data-dependent noise. Based on this simplification, analysis of linear equalization and optimum detection have been done in [34, 37].

We may also derive an approximate model for (3.4), however, using a different approach. Recall from Section 2.1.1 that the bit response is the convolution of the channel impulse response $h_i(t)$ with the impulse response $\tilde{p}(t)$ of the write circuit. Therefore, we can express $h_{b,m}(t)$ as

$$h_{b,m}(t) = h_i(t) \otimes \tilde{p}_m(t) \tag{3.7}$$

where $\tilde{p}_m(t)$ is an ideal rectangular pulse of duration T_m (instead of T) and ampli-

tude 1.0. Therefore, the Fourier transform of $h_{b,m}(t)$ can be expressed as

$$H_{b,m}(f) = H_i(f)\tilde{P}_m(f) \tag{3.8}$$

where $H_i(f)$ and $\tilde{P}_m(f)$ are the Fourier transforms of $h_i(t)$ and $\tilde{p}_m(t)$, respectively, with

$$\tilde{P}_m(f) = T_m \frac{\sin(\pi f T_m)}{\pi f T_m} e^{-j\pi f T_m}. \tag{3.9}$$

At high densities, much of the energy in $H_i(f)$ is contained well within the null-to-null bandwidth of $\tilde{P}_m(f)$. Therefore, we may approximate $H_{b,m}(f)$ as [27]

$$H_{b,m}(f) \approx T_m \frac{\sin(\pi f T)}{\pi f T} H_i(f) e^{-j\pi f T}, \tag{3.10}$$

whose time-domain equivalent is

$$h_{b,m}(t) \approx \frac{T_m}{T} h_b(t). \tag{3.11}$$

Substituting (3.11) in (3.4), we obtain

$$r_n \approx \sum_m \tilde{a}_m h_b(nT - mT - \Delta_m) + v_n \tag{3.12}$$

where

$$\tilde{a}_m = a_m \frac{T_m}{T}. \tag{3.13}$$

Thus, the approximation amounts to a multiplicative change in the bit-amplitude and a shift in the bit-position, while the bit response is computed based on the bit-duration T. The model in (3.12) may be further approximated using Taylor

expansion to derive a model similar to (3.6) as

$$r_n \approx \sum_m \tilde{a}_m h_b(nT - mT) - \sum_m \tilde{a}_m \Delta_m \tilde{h}_i(nT - mT) + v_n \tag{3.14}$$

where

$$\tilde{h}_i(t) = \frac{\partial h_b(t)}{\partial t} = h_i(t) - h_i(t - T). \tag{3.15}$$

Comparing the approximations made in deriving (3.6), (3.12) and (3.14), we can see that the approximate model (3.12) will be more accurate compared to (3.6) and (3.14) for large jitter.

The simplified models are acceptable only when the standard deviation σ_Δ of jitter is small enough compared to the bit duration T. But, the jitter becomes quite large at high densities, thus making the simplified models inaccurate. Hence in this chapter, we focus on the media noise problem based on the channel model (3.2), which gives a clearer and accurate picture of the effect of media noise on the readback signal without any approximations. Even though the exact models given by (3.2) and (3.4) are equivalent, we choose (3.2) for our study in this chapter since it leads to some ease in theoretical analysis compared to (3.4), as explained at the end of Section 3.2.1.

In this chapter, we use the hyperbolic tangent function based perpendicular magnetic recording channel, given in Section 2.1.1 (see Eq.(2.9)).

3.2 Optimum Joint Target and Equalizer Design

Figure 3.1 shows the block schematic used for the joint design of the GPR target $G(z)$ and equalizer $W(z)$. For this design, we use the widely used MMSE approach, that is, by minimizing $E[e_n^2]$ where $E[\cdot]$ denotes the expectation operator. The

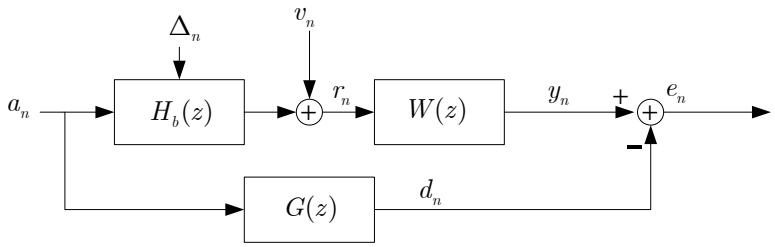

Figure 3.1: Joint PR equalizer and target design for channels with jitter noise.

equalizer output y_n and target output d_n are given by

$$y_n = \mathbf{w}^T \mathbf{r}_n \quad \text{and} \quad d_n = \mathbf{g}^T \mathbf{a}_n, \tag{3.16}$$

where superscript 'T' denotes transpose, $\mathbf{w} = [w_{-K}, w_{-K+1}, \cdots, w_{K-1}, w_K]^T$ is the equalizer with length $N_w = 2K + 1$, $\mathbf{g} = [g_0, g_1, \cdots, g_{N_g-1}]^T$ is the target with length N_g, $\mathbf{r}_n = [r_{n+K}, r_{n+K-1}, \cdots, r_{n-K}]^T$, $\mathbf{a}_n = [a_n, a_{n-1}, \cdots, a_{n-N_g+1}]^T$, and the positive integer K accounts for the delay from channel input to equalizer output[1]. First we review the results for recording channels without media noise. Thereafter, we introduce a new cost function for channels with media noise and derive the expressions required for computation of the statistics required for designing the optimum equalizer and target.

For the channel without media noise, the mean square error (MSE) at the equalizer output is given by [35]

$$E[e_n^2] = \mathbf{w}^T \mathbf{R} \mathbf{w} + \mathbf{g}^T \mathbf{A} \mathbf{g} - 2\mathbf{w}^T \mathbf{P} \mathbf{g}, \tag{3.17}$$

where $\mathbf{R} = E[\mathbf{r}_n \mathbf{r}_n^T]$ is a $N \times N$ auto-correlation matrix of the channel output r_n, $\mathbf{A} = E[\mathbf{a}_n \mathbf{a}_n^T]$ is a $N_g \times N_g$ auto-correlation matrix of the input data a_n, and $\mathbf{P} = E[\mathbf{r}_n \mathbf{a}_n^T]$ is a $N \times N_g$ cross-correlation matrix between r_n and a_n.

To minimize the MSE in (3.17) while avoiding the trivial solution $\mathbf{g} = \mathbf{0}$ and

[1]In Chapter 2, we accounted for the delay parameter K in the target path in Figure 2.5. Making the equalizer noncausal as in Figure 3.1 is equivalent to this.

$\mathbf{w} = \mathbf{0}$, some constraint needs to be imposed. The widely used monic-constraint (*i.e.* $g_0 = 1$) has noise whitening ability since it results in an equalizer that is equivalent to the forward equalizer of the MMSE solution of decision feedback equalization [57]. Hence we focus on the design problem using monic-constraint in this chapter.

The results of the monic constrained MMSE design for channels without media noise are given by [35]

$$\lambda = \frac{1}{\mathbf{i}^T(\mathbf{A} - \mathbf{P}^T\mathbf{R}^{-1}\mathbf{P})^{-1}\mathbf{i}}, \tag{3.18}$$

$$\mathbf{g} = \lambda(\mathbf{A} - \mathbf{P}^T\mathbf{R}^{-1}\mathbf{P})^{-1}\mathbf{i}, \tag{3.19}$$

$$\mathbf{w} = \mathbf{R}^{-1}\mathbf{P}\mathbf{g}, \tag{3.20}$$

where λ is the Langrange multiplier and $\mathbf{i} = [1, 0, 0, \cdots, 0]^T$ is a vector of length N_g.

Now we consider the channel model with jitter noise as shown in Figure 3.1. Since jitter noise is data-dependent and non-stationary, the optimum equalizer and target should also be data-dependent and hence time-variant, which may require unaffordable complexity. Also, any statistical computation done on the channel output will need to incorporate the data-dependence of media noise. On the other hand, prior to Viterbi detection, we have no idea about the recorded bit sequence and thus we can not know what are the specific noise characteristics that must be used for designing the equalizer and target for each instant. Therefore, we use the following approach to circumvent these issues. We use the squared error averaged over all possible recorded sequences as our cost function to minimize, which is given by

$$\xi_{\text{MSE}} = \sum_{\bar{\mathbf{b}}} E[e_n^2|\bar{\mathbf{b}}] \Pr(\bar{\mathbf{b}}), \tag{3.21}$$

where $\{\bar{\mathbf{b}}\}$ denotes any possible recorded sequence. Note that this cost func-

tion combines ISI, electronics noise and media noise into one function. At the same time, this cost function accounts for the data-dependent nature of the media noise, with the sequences that result in more jitter noise (*i.e.* more transitions) receiving more weightage in the cost function, and vice versa. Thus, even though the cost function ξ_{MSE} and the resulting optimum equalizer and target are data-independent, the construction of the cost function ensures that the optimum solution is implicitly tuned to respond to the different data sequences in accordance with the amounts of jitter noise caused by these sequences.

Based on this new cost function, it is straight-forward to see that the optimum equalizer and target are still given by (3.18)-(3.20) except that the matrices $\mathbf{R}$, $\mathbf{P}$ and $\mathbf{A}$ are now defined as

$$\bar{\mathbf{R}} = \sum_{\bar{\mathbf{b}}} E[\mathbf{r}_n \mathbf{r}_n^T|_{\bar{\mathbf{b}}}] \Pr(\bar{\mathbf{b}}), \tag{3.22}$$

$$\bar{\mathbf{P}} = \sum_{\bar{\mathbf{b}}} E[\mathbf{r}_n \mathbf{a}_n^T|_{\bar{\mathbf{b}}}] \Pr(\bar{\mathbf{b}}), \tag{3.23}$$

$$\bar{\mathbf{A}} = \sum_{\bar{\mathbf{b}}} E[\mathbf{a}_n \mathbf{a}_n^T|_{\bar{\mathbf{b}}}] \Pr(\bar{\mathbf{b}}). \tag{3.24}$$

In this chapter, we assume all the data patterns to be equally probable. Hence, we have $\bar{\mathbf{A}} = \mathbf{A}$. Computation of the conditional statistics required for $\bar{\mathbf{R}}$ and $\bar{\mathbf{P}}$ is not a trivial numerical problem and is the major task here. There arise some issues in this numerical computation process caused by the channel model in (3.2), which are discussed below.

3.2.1 Truncation of the Step Response

The step response of perpendicular recording channel has infinite length and hence we need to truncate it while doing simulations. When truncating the step response, we should ensure that there does not arise any instability or inaccuracy due to

truncation. Since the step response given by (2.9) does not tend to zero at positions far from the transition position, we cannot simply truncate the step response to some range around $t = 0$.

By comparing the step response and bit response, we can solve the truncation problem. When we use truncated bit response for simulating perpendicular magnetic recording channels, it works fine because the tails of bit response tend to zero at positions far from the bit position. However, underlying this approach is a hidden assumption that the input bits before the first bit and after the last bit are 0. This means that we should have transitions with level $+1$ or -1 at the starting bit position and the ending bit position of the data pattern, whereas the transition levels inside the data pattern are $+2$,-2 or 0. Therefore, if we add two extra transitions with levels $+1$ or -1 at the two ends of the transition sequence according to the bits recorded, we can use step response to do simulations instead of bit response. With this change, we can now truncate the step response such that it reaches saturation on both sides and the length on each side is greater than the length of the data pattern under consideration.

In the absence of jitter noise, it can be shown that the truncation of step response is equivalent to truncation of bit response, and hence either step response or bit response can be used in simulations and computations. When jitter noise is present, we prefer to use step response instead of bit response because the responses due to different transitions are independent given a data pattern while this property does not hold for bit response (see (3.2)-(3.5)).

3.2.2 Computation of Matrices $\bar{\mathbf{R}}$ and $\bar{\mathbf{P}}$

To get the optimum solution, we need to compute the correlation matrices $\bar{\mathbf{R}}$ and $\bar{\mathbf{P}}$ given by (3.22) and (3.23), respectively. Clearly these can only be obtained through numerical computations since there are no closed-form expressions.

In jitter noise dominated high-density perpendicular recording channels, the matrix $\bar{\mathbf{R}}$ is found to be highly ill-conditioned with some of its eigenvalues close to zero. Hence, it is important to avoid numerical inaccuracy as much as possible. Therefore, instead of resorting to data-averaging to estimate the conditional correlations, we developed a rigorous analytical approach and the solution of which can be computed numerically. The detailed computation process is as follows.

First of all, we note that by defining the cost function ξ_{MSE} in (3.21) as the averaged squared error over all possible data patterns, the data-dependence and associated non-stationarity caused by jitter noise are taken care of. In other words, the data-dependent averaging converts the underlying non-stationary problem into a wide-sense stationary problem[2]. As a result, the matrix $\bar{\mathbf{R}}$ is a toeplitz symmetric matrix. Therefore, to compute $\bar{\mathbf{R}}$, we only need to develop the expression for $E[r_k r_{k-n}]$, where $\{r_n\}$ is the equalizer input given by (3.2). From (3.22), we get

$$E[r_k r_{k-n}] = \sum_{\bar{\mathbf{b}}} E[r_k r_{r-n}|\bar{\mathbf{b}}] \Pr(\bar{\mathbf{b}}). \tag{3.25}$$

For the sake of convenience, we shall re-write (3.2) as

$$r_k = \tilde{r}_k + v_k = \sum_i b_i h(i,k) + v_k \tag{3.26}$$

where $\tilde{r}_k$ denotes the signal without including the electronics noise and $h(i,k) \triangleq h_s(kT - iT + \Delta_i)$ denotes the step response at the position kT due to the transition at position iT. Therefore, we get

$$E[r_k r_{k-n}] = \tilde{\phi}_{k,n} + \sigma_v^2 \delta_n \tag{3.27}$$

[2]This statement is true only if the data $\{a_n\}$ is wide-sense stationary.

where

$$\tilde{\phi}_{k,n} = E[\tilde{r}_k \tilde{r}_{k-n}] = \sum_{\bar{\mathbf{b}}} \sum_{i,j} E[b_i h(i,k) b_j h(j,k-n)|\bar{\mathbf{b}}] \Pr(\bar{\mathbf{b}}), \tag{3.28}$$

with $\delta_k = 1$ if $k = 0$ and $\delta_k = 0$ if $k \neq 0$.

When $i \neq j$, $h(i,k)$ and $h(j,k-n)$ are independent, because the transition jitters at different positions are independent. Thus we need to compute $E[h(i,k)|\bar{\mathbf{b}}]$ and $E[h(j,k-n)|\bar{\mathbf{b}}]$ using the probability density function (pdf) of the transition jitter. The effect of conditioning with data pattern $\bar{\mathbf{b}}$ in $E[h(i,k)|\bar{\mathbf{b}}]$ is to know whether or not there is a transition at position iT. When $i = j$, $h(i,k)$ and $h(j,k-n)$ are dependent since they contain the same transition jitter at position iT. Then we need to compute $E[h(i,k)h(i,k-n)|\bar{\mathbf{b}}]$. Since we assumed that each data pattern is equally probable, we obtain

$$\tilde{\phi}_{k,n} = \frac{1}{2^{L_d-1}} \sum_{\bar{\mathbf{b}}} \sum_{i,j} E[b_i h(i,k) b_j h(j,k-n)|\bar{\mathbf{b}}] \tag{3.29}$$

where L_d is the length of transition sequences considered.

Since each recorded bit is equally probable to be $+1$ or -1, we can compute the probability distributions of $\{b_i\}$. It can be easily shown that

$$\Pr[b_i = 2] = \Pr[b_i = -2] = 1/4 \tag{3.30}$$

$$\Pr[b_i = 0] = 1/2 \tag{3.31}$$

$$\Pr[b_{i+1}|b_i = 0] = \Pr[b_{i+1}] \tag{3.32}$$

$$\Pr[b_{i-1}|b_i = 0] = \Pr[b_{i-1}] \tag{3.33}$$

$$\Pr[b_{i+1} = -b_i|b_i \neq 0] = \Pr[b_{i+1} = 0|b_i \neq 0] = 1/2 \tag{3.34}$$

$$\Pr[b_{i-1}|b_i \neq 0] = \Pr[b_{i+1}|b_i \neq 0] \tag{3.35}$$

and the transitions which are not neighbouring to each other are independent. Hence, substituting (3.30)-(3.35) in (3.29), we get

$$\begin{aligned}
\tilde{\phi}_{k,n} &= \frac{1}{2^{L_d-1}} \sum_{\bar{\mathbf{b}}} \sum_{i} \sum_{j=i-1}^{i+1} E[b_i b_j h(i,k) h(j,k-n) | \bar{\mathbf{b}}] \\
&= \frac{1}{2^{L_d-1}} \sum_{\bar{\mathbf{b}}} \sum_{i} \sum_{j=i-1}^{i+1} b_i b_j E[h(i,k) h(j,k-n) | \bar{\mathbf{b}}] \\
&= 2 \sum_{i} E[h(i,k) h(i,k-n)] \\
&\quad - \sum_{i} E[h(i,k)\} E[h(i-1,k-n)] \\
&\quad - \sum_{i} E[h(i,k)] E[h(i+1,k-n)]. \qquad (3.36)
\end{aligned}$$

Thus we see from (3.36) that we do not need to compute the autocorrelation matrices for each data pattern and sum them up. Instead, we only need to compute $E[h(i,k)]$ and $E[h(i,k)h(i,k-n)]$ for the transition at position iT. Thus, possible numerical inaccuracy is highly minimized. Note that $E[h(i,k)]$ is only a function of $k-i$, and $E[h(i,k)h(i,k-n)]$ is a function of $k-i$ and $k-n-i$.

Another thing to note is that each data pattern must start and end with transitions with amplitude $+1$ or -1. In other words, b_1 and b_{L_d} are equally probable to be $+1$ or -1. Thus, the summations in (3.36) will be modified slightly when i is equal to 1 and L_d. Doing this, we get

$$\begin{aligned}
\tilde{\phi}_{k,n} &= E[h(1,k)h(1,k-n)] + E[h(L_d,k)h(L_d,k-n)] \\
&\quad + 2 \sum_{i=2}^{L_d-1} E[h(i,k)h(i,k-n)] - \sum_{i=2}^{L_d} E[h(i,k)] E[h(i-1,k-n)] \\
&\quad - \sum_{i=1}^{L_d-1} E[h(i,k)] E[h(i+1,k-n)]. \qquad (3.37)
\end{aligned}$$

Similarly, we can obtain the $(p,q)^{\text{th}}$ element of $\bar{\mathbf{P}}$ as

$$\begin{aligned}\bar{P}_{p,q} &= \sum_{\bar{\mathbf{b}}} E[r_{n+K-p}a_{n-q}|_{\bar{\mathbf{b}}}]\Pr(\bar{\mathbf{b}}) \\ &= \sum_{\bar{\mathbf{b}}}\sum_{i} E[h(i,n+K-p)b_i a_{n-q}|_{\bar{\mathbf{b}}}]\Pr(\bar{\mathbf{b}}) \\ &= E[h(n-q,n+K-p)] - E[h(n-q+1,n+K-p)]. \qquad (3.38)\end{aligned}$$

Thus, given the channel step response, jitter pdf and electronics noise power, we can accurately compute the correlation matrices $\bar{\mathbf{R}}$ and $\bar{\mathbf{P}}$.

3.3 Computational and Simulation Results

As an example, we show here the computational results under the following conditions:

(1)Perpendicular magnetic recording, (2)Effective length of truncated step response is 40 bits, (3)Equalizer length $N_w = 15$, (4)Target length $N_g = 5$, (5)Linear density $D_c = 2.0$, (6)Monic-constraint for target response, (7)Range of transition jitter is from $\sigma_\Delta/T = 0\%$ to $\sigma_\Delta/T = 10\%$, (8)At least 1000 error bits are collected for every estimate of the bit error rate (BER). Conventional Viterbi detector (VD) with no modifications is used for data detection. The strength of the additive white Gaussian electronics noise (AWGN) v_n is chosen according to the signal to noise ratio (SNR) defined in Chapter 2 (see Eq.(2.10)). Thus, our SNR definition includes only the electronics noise.

The optimum GPR targets designed under different jitter variances are shown in Figure 3.2. The SNR used in this design is 35 dB for all cases. Observe that the effective target length decreases with increase in jitter. In fact, with 10% jitter, the optimum target uses only 4 out of the 5 taps provided. Further, the slopes of

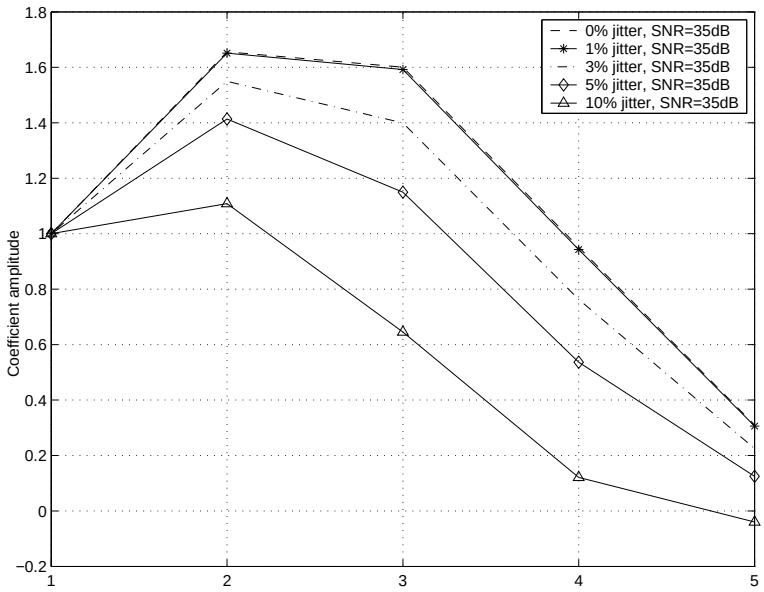

Figure 3.2: Optimal target responses obtained for recording channel with jitter.

the target at the sampling points as well as the bandwidth of the target are seen to progressively decrease with increase in jitter percentage. These charactersitics are very desirable to minimize the amount as well as effect of jitter noise at detector input. Similar observations were reported earlier for longitudinal recording in [35, 37]. It is also important to note that the target energy keeps decreasing with increase in jitter, thereby predicting severe degradation in the performance of VD.

In the MMSE and BER performances given in Figures. 3.3 to 3.5, the equalizer and target are re-optimized for each SNR. Figure 3.3 shows the MMSE, normalized by the target energy, for different amounts of jitter. Also shown, for the sake of comparison, is the normalized MSE computed for 5% jitter channel using the equalizer and target designed for jitter-free case. This curve lies below the MMSE curve corresponding to 5% jitter channel with corresponding optimum equalizer and target since the target energy for the jitter-free channel is much higher than the target energy for 5% jitter channel[3], as can be seen from Figure 3.2. What

[3]If we examine the unnormalized MSE plots corresponding to Figure 3.3, we will find that the MSE computed for 5% jitter channel using equalizer and target optimized for jitter-free case

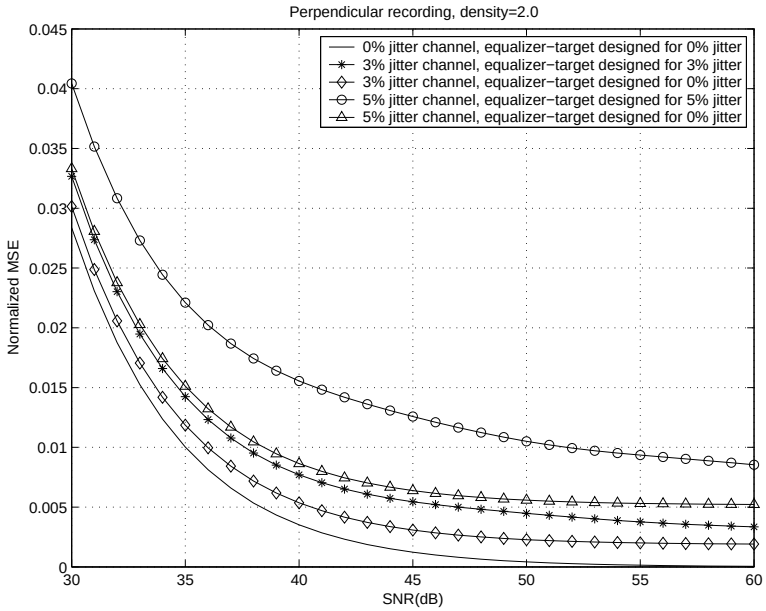

Figure 3.3: Normalized MMSE obtained for recording channel with jitter.

is important to note is that the target optimized for jitter-free case results in an error-floor in the MSE curve when used on jitter channels. This will lead to similar error-floor effect in BER performance too. On the other hand, targets optimized for jitter channels result in monotonically decreasing MMSE, thereby implying that these targets help to delay the onset of error-floor to much higher SNR values. As the slopes of these MMSE curves approach zero, we can expect the error-floor to manifest.

To have a clear idea of the effectiveness of the joint target and equalizer design, we need to check the BER performance of VD using the targets and equalizers obtained. Figure 3.4[4] shows the BER performances using different target responses and linear equalizers for 3% jitter. Since [1 2 3 2 1] is a widely used standard target for perpendicular channels [41], we also include the performance of VD with fixed target [1 2 3 2 1] for the purpose of comparison. The detection performance of

is the highest for all SNRs, which is quite expected. Furthermore, this MSE has its minimum at SNR=44dB and increases monotonically as SNR is further reduced or increased from 44dB.

[4]Note that the BER range of interest here is around 10^{-3} to 10^{-5}, hence we focus on the SNR regions higher than 30 dB.

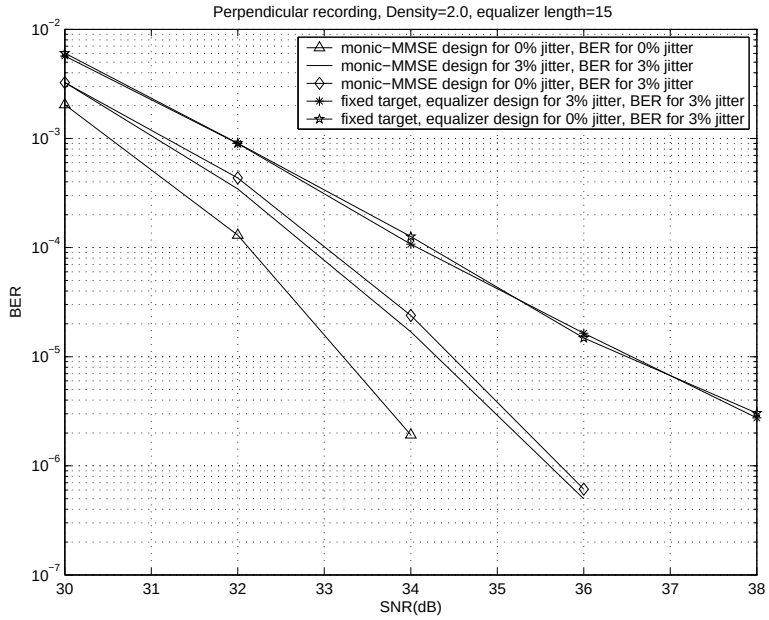

Figure 3.4: BER comparison between designed target responses and fixed target [1 2 3 2 1] for 3% jitter.

VD on a jitter-free channel using a monic-constrained GPR target designed for 0% jitter is included in Figure 3.4 to serve as a reference for assessing the performance for other targets. First of all, we note that the performance of fixed target remains the same whether or not jitter noise is accounted for in the equalizer design. This shows that the choice of target is highly critical in media noise channels, even as was observed in [37]. It is also clear from Figure 3.4 that the BER plots for the fixed target are showing indications of error-floor even as early as 36-38dB. Compared to this, the monic-constrained GPR targets improve the performance significantly for channels with jitter, and that too with no indication of error-floor. However, we note that the performance of the GPR target which is optimized for the jitter channel is not significantly better than that of the GPR target which is optimized for jitter-free channel, the gain being just about 0.2-0.3dB. This is mainly because 3% jitter is not large enough to make the overall channel noise strongly data-dependent in nature, for the range of SNRs considered here. However, we can expect the effect of jitter to show up if we do the simulation at much higher SNRs. The simulation conditions chosen for Figure 3.5 help to verify this conjecture.

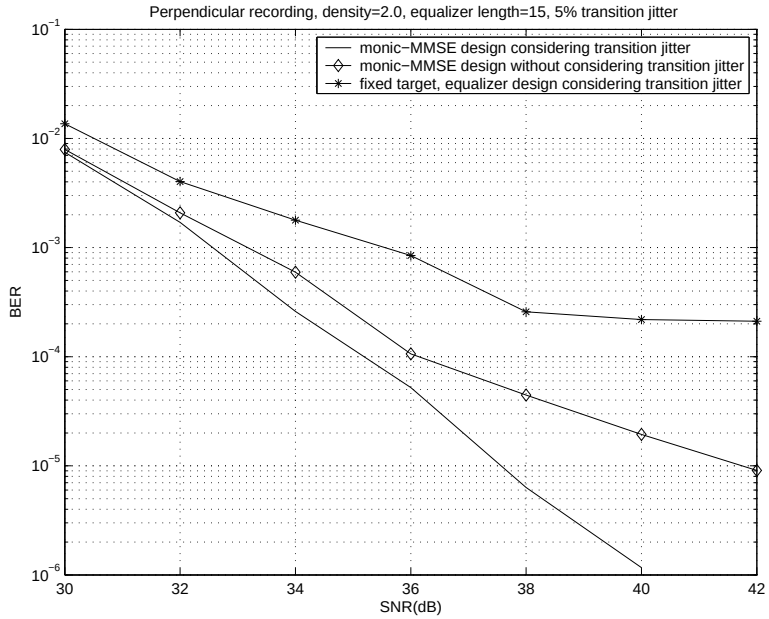

Figure 3.5: BER comparison between designed target responses and fixed target [1 2 3 2 1] for 5% jitter.

Figure 3.5 shows the BER performance comparison results for channels with 5% jitter. The advantage of the proposed joint design approach is clearly manifest in this figure. In particular, the region of interest to us in this chapter is the very high SNR region where jitter noise is dominant. In this region, the proposed design approach provides significant improvement in performance while the other targets exhibit error-floor effect. While the fixed target [1 2 3 2 1] is not even able to reach a BER of 10^{-4}, the GPR target designed without considering jitter seems to level off to a BER of 10^{-5}. On the other hand, even at 40dB, there is not yet an indication of the onset of error-floor for the proposed approach. Thus we see that the onset of error-floor is much delayed by the GPR target whose design incorporates the jitter compared to all the other targets.

3.4 Additional Comments

We shall now comment on some specific aspects of the work reported in this chapter, with the objective of highlighting the distinctiveness of our work from already published work.

First we comment on the importance of numerical accuracy in the computation of $\bar{\mathbf{R}}$ and $\bar{\mathbf{P}}$ in Section 3.2.2. Actually, $\bar{\mathbf{R}}$ and $\bar{\mathbf{P}}$ can also be estimated through data-averaging over a sufficiently large sequence of channel output samples $\{r_n\}$. But, the matrix $\bar{\mathbf{R}}$ for jitter dominated perpendicular recording channel turns out to be highly ill-conditioned. Therefore, since the design equations (3.18) to (3.20) include matrix inversion operations, any small inaccuracy in $\bar{\mathbf{R}}$ tends to result in serious impact on the performance. Consequently, the number of samples of r_n needed to keep the estimation error very small becomes excessively large to be of practical use. On the other hand, by using the expressions developed in this chapter, we can accurately compute $\bar{\mathbf{R}}$ with very minimum computational and memory requirements. We may also point out that the use of first-order model given in (3.6) does not lead to an ill-conditioned $\bar{\mathbf{R}}$. Since all the existing studies are based on models of the type (3.6), the problem of numerical inaccuracy in the estimation of $\bar{\mathbf{R}}$ was not encountered.

We choose to use the channel model (3.2) instead of (3.6) in our computations and simulations in this chapter, since (3.2) is more accurate for high-density recording with transition jitter in the range of 5% to 10%. In fact, for such high jitter, the first-order model in (3.6) can be grossly in error and the conclusions drawn based on studies conducted using this model can be misleading. Based on the channel model (3.2), we also give a rigorous approach to do computations and simulations using step response instead of bit response. To our knowledge, no work has been reported in the past on deriving analytical expressions for computing the correlations using the exact model (3.2). There have also been no remarks in existing

publications on how to do simulation using the exact model (3.2) for perpendicular recording channels where the underlying step response is of infinite duration. We also developed a bit response based exact model given by (3.4) for simulating jitter noise channel. This model makes the simulation effort even easier compared to the step response based model in (3.2). Further, the approximate model (3.12), which we developed based on (3.4), is more accurate than the first-order model in (3.6).

The cost function (3.21) used in this chapter accounts for the data-dependence of media noise in an implicit way even though the expression is data-independent. It can be seen that sequences with more transitions, which result in more significant jitter noise effect, will have larger weightage in the cost function, and vice versa. Thus, the proposed cost function results in a good compromise between hardware complexity and performance, as an explicitly data-dependent equalizer-target approach would result in unaffordable complexity levels.

There have been publications on analytical approaches for the design of GPR target [37, 45]. But, these approaches are based on infinite length equalizers (*i.e.* joint design of infinite-length equalizer and finite-length target), even though these may be replaced/approximated by finite-length equalizers after getting the target. On the other hand, our proposal is for joint design of equalizer and GPR target where both the equalizer and target are of finite-length.

In this chapter, the SNR definition (2.10) includes only the electronics noise, and the effect of transition jitter is measured by the ratio σ_Δ/T. This is similar to the approach used in [25,57]. On the other hand, several papers use a different SNR definition where the noise power is taken as the sum of the powers of electronics noise and jitter noise, with the jitter noise power computed based on either single transition or multiple transitions [32, 41, 45]. Since jitter noise and electronics noise have very different effect on the detection performance, defining the SNR by adding the powers of these noises may lead to inconsistent results. For example,

the detection performance for a given SNR could be quite different for two different compositions (*e.g.* 25:75, 75:25) of the two noises. For this reason, we choose to use only the electronics noise in defining the SNR.

Finally, note that our proposal in this chapter is only for designing optimum equalizer and target. We did not propose any modifications to the detector. On the other hand, there have been several proposals for developing optimum or sub-optimum detectors for jitter noise channels, as we reviewed in Section 1.4.2. Our method is complementary to these proposals for detector modifications. Therefore, the equalizer and target designed using our approach can be combined with any of these detection approaches to result in even better performance for data detection in the presence of jitter noise. In fact, in Chapter 4, we address the problem of detector modifications for channels with jitter noise.

3.5 Conclusions

In this chapter, we considered high-density perpendicular magnetic recording channels with jitter noise and proposed a novel approach to jointly design optimum generalized partial response target and linear equalizer. We investigated the problem using a step response based channel model without making any approximations and derived analytical expressions for the statistics required to obtain the optimum target response and equalizer through minimizing a new MMSE-based cost function. The resulting GPR targets provide significant gain over targets which are designed without considering jitter noise. In particular, the GPR targets designed using the proposed cost function significantly delay the onset of error-floor in the detection performance compared to other targets.

Chapter 4

A Novel Post-Processing Approach for Signal Detection in Channels with Jitter Noise

In this chapter, we present a novel post-processing approach for signal detection in high-density magnetic recording channels with transition jitter. We start with comparing the complexities and BER performances of two sequence detection approaches with data-dependent mean/variance compensation for the channel noise and data-dependent noise prediction, respectively, with normal Viterbi detector (VD). Thereafter, we propose a two-step post-processing approach for signal detection to combat the jitter noise. The post-processing approach improves the BER performance of VD significantly with minor increase in computational complexity. Performance analysis and simulation results are also presented.

4.1 Motivation

In Chapter 3, we presented the design of optimum PR targets and equalizers for high-density magnetic recording channels with jitter noise. The GPR targets and equalizers are shown to be able to effectively reduce the degradation in detection performance caused by transition jitter. However, we observe that (see Figure 3.4)

the BER performance is still worse than the case without transition jitter. This means that media noise is still a major disturbance in the channel, and it motivates us to investigate further approaches to combat media noise combined with the GPR targets and equalizers designed in Chapter 3.

We look into signal detection approaches that account for the data-dependence of media noise. As mentioned in Section 1.4.2, there are some optimum detection approaches to combat media noise. The pattern-dependent noise-predictive ML detection approach in [34] and the optimum sequence detection approach using optimized branch metrics in [23] are essentially equivalent. A simpler approach is to account for the data-dependent mean and variance of media noise in the branch metrics of normal VD [46, 58]. However, the computational complexity of these approaches is much higher than that of normal VD, and this is the main obstacle in using these approaches in practical hard drive systems. Hence, in this chapter, our objective is to develop new approaches that have close-to-optimum performance with moderate increase in complexity.

4.2 Existing Signal Detection Approaches to Combat Media Noise

In this section, we compare the complexity and performances of three existing detection approaches, which are the normal VD, VD with mean/variance compensation for media noise (VD-MV), and VD with data-dependent noise prediction (VD-NP).

4.2.1 Computational Complexity

The trellis search algorithms for the three different detection approaches mentioned above (*i.e.*, normal VD, VD-MV and VD-NP) are essentially the same except that

the branch metric definitions are different. Thus, we only need to compare the computation of branch metrics in the three cases. To make a fair comparison and for simplicity, we assume that the number of states in the trellis is same for all the three detection approaches.

A. Normal VD

For normal VD, as introduced in Chapter 2, the assumption is that the noise is AWGN. Therefore, the branch metric at time n for any branch in the trellis is

$$BM_{VD,n} = |y_n - \tilde{d}_n|^2 \tag{4.1}$$

where y_n is the actual equalizer output (or VD input) at instant n and $\tilde{d}_n = \sum_{i=0}^{N_g-1} g_i \tilde{a}_{n-i}$ is the noiseless output value corresponding to the n^{th} branch on the particular trellis path defined by the data sequence $\{\tilde{a}_n\}$. Thus, computation of the branch metric requires one subtraction and one multiplication. Here, we have assumed that the noiseless outputs $\tilde{d}_n$ are computed before-hand and can be retrieved from a look-up table.

B. VD-MV

Since media noise is data-dependent, we can modify the branch metric definition in VD to compensate for the data-dependent mean and variance of the noise samples [46, 58]. The new branch metric is defined as

$$BM_{VD-MV,n} = \frac{|y_n - \tilde{d}_n - m_n|^2}{\sigma_n^2} + \ln \sigma_n^2 \tag{4.2}$$

where m_n and σ_n^2 are the mean and variance, respectively, of the noise samples which are dependent on the data pattern[1] $[\tilde{a}_n, \tilde{a}_{n-1}, \cdots, \tilde{a}_{n-N_g+1}]$. Hence, computation of the branch metric requires three additions/subtractions, one multiplication, one division and one logarithm.

C. VD-NP

Since the noise samples are data-dependent and correlated, we could make an estimation of the current noise sample in y_n based on the past noise samples by means of linear prediction, where the predictor coefficients are dependent on the data-pattern under consideration on the trellis path. To do this, we would need to incorporate a bank of data-dependent noise predictors in the normal VD [34]. The linear predictors can be designed based on minimum mean square error (MMSE) criterion for each data pattern. We get the modified branch metric in the trellis as

$$BM_{VD-NP,n} = \frac{|y_n - \tilde{d}_n - \hat{e}_n|^2}{\tilde{\sigma_n}^2} + \ln \tilde{\sigma_n}^2 \tag{4.3}$$

where $\hat{e}_n = \sum_{i=n-N_p}^{n-1} e_i f_{n-i}$ is the estimated noise sample corresponding to path $\{\tilde{a}_n\}$ at n^{th} branch, N_p is the order of the predictor, $[f_1, f_2, \cdots, f_{N_p}]$ are the predictor coefficients, $e_n = y_n - \tilde{d}_n$ is the noise sample at n^{th} branch on path $\{\tilde{a}_n\}$, and $\tilde{\sigma}_n^2$ is the variance of the residual noise $e_n - \hat{e}_n$ at the predictor output. Note that $e_{n-1}, e_{n-2}, \cdots, e_{n-N_p}$ are determined by the survivor path associated with the current branch under consideration. Thus, computation of the branch metric requires $N_p + 2$ additions/subtractions, $N_p + 1$ multiplications, one division and one logarithm.

In Table 4.1, we summarize the computational complexities of the three differ-

[1]Strictly speaking, the span of data-dependence need not be limited to $[\tilde{a}_n, \tilde{a}_{n-1}, \cdots, \tilde{a}_{n-N_g+1}]$. Since considering a longer span would lead to exponential increase in trellis size and the associated computations, we restrict the data-dependence span to $[\tilde{a}_n, \tilde{a}_{n-1}, \cdots, \tilde{a}_{n-N_g+1}]$.

Table 4.1: Complexity comparison of branch metric computations for the three detection approaches VD, VD-MV and VD-NP.

	$+/-$	$\times$
Normal VD	1	1
VD-MV	3	2
VD-NP	$N_p + 2$	$N_p + 2$

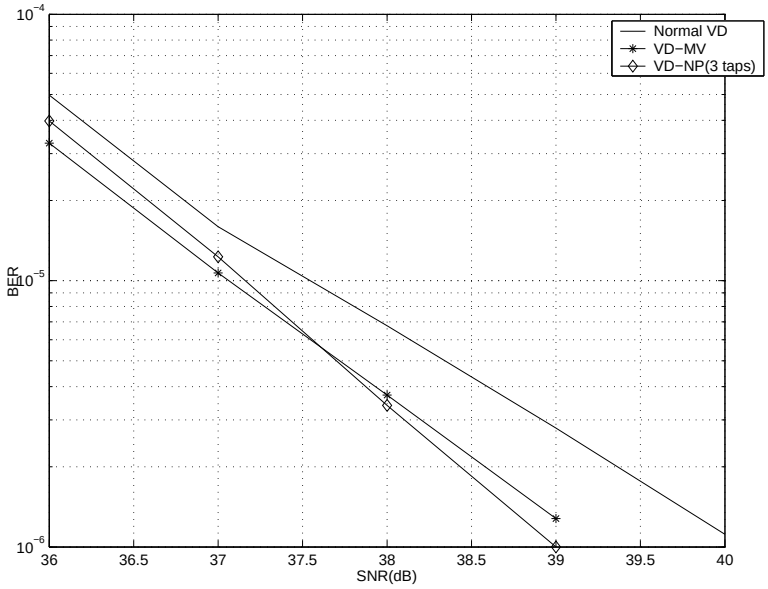

Figure 4.1: BER performances of three different detection approaches.

ent detection approaches. It shows that the complexity of VD-MV and VD-NP is much higher than that of normal VD.

4.2.2 BER Performance

Since VD-MV and VD-NP incorporate the data-dependent characteristics of the media noise, their resulting BER performances should be better than that of normal VD. We did some simulations using the 5-tap GPR targets designed in Chapter 3. The SNR is defined as (2.10). Figure 4.1 shows the BER performances of the three different detection approaches for 5% jitter channel, N_p is set to 3 for VD-NP, and at least 1000 error bits are collected for each estimate of BER. The data-dependent mean and variance used in VD-MV are estimated through

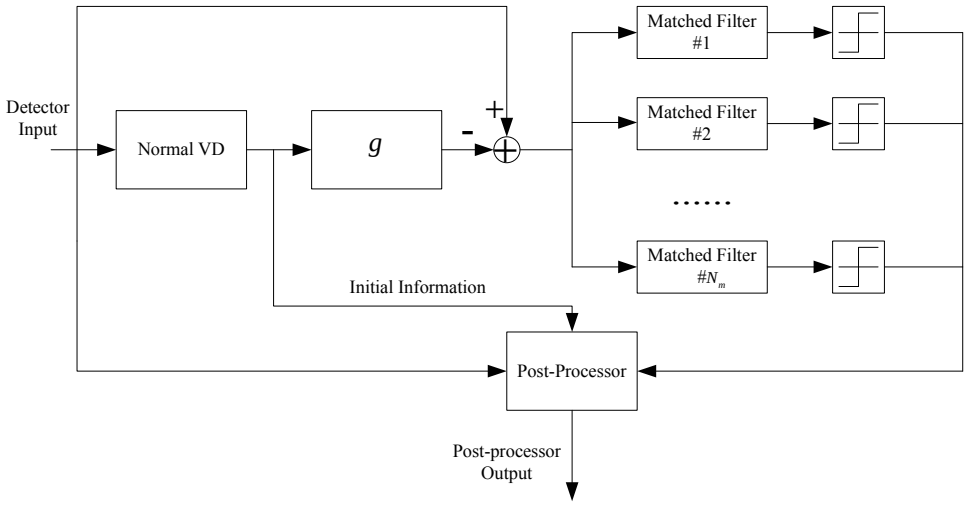

Figure 4.2: Schematic of the two-step post-processing approach.

collecting a large number of noise samples for each data pattern (here, we collect over 1.2×10^5 noise samples for each data pattern and it is observed that the estimated values have converged well). Similarly, we obtain the data-dependent noise characteristics that are used to design the data-dependent noise predictors [34]. Figure 4.1 shows that the gain of VD-MV and VD-NP over normal VD is about 1dB at BER of 10^{-6}.

In summary, using VD-MV or VD-NP instead of normal VD, we can improve the BER performance by about 1dB at the cost of much higher complexity. This motivates us to explore the development of detection approaches that offer better trade-offs between BER performance and computational complexity.

4.3 A Two-step Post-processing Approach

To improve the BER performance while avoiding the complexity increase, we present a novel two-step post-processing approach in this section. The first step is to identify all the possible error regions from the normal VD output using a simple threshold-based approach, and the second step is to re-detect only these

regions using approaches that incorporate the data-dependent characteristics of jitter noise. Thus, the complexity increase is mostly limited to the post-processing regions, which are quite short in length.

4.3.1 First Step: Identifying the Possible Error Regions

To identify the possible error regions in the output of normal VD, we generate a reference signal by passing the output sequence of the normal VD through the ideal channel whose bit response is the GPR target. Next, we subtract the reference signal from corresponding real detector input signal, getting

$$\bar{e}_n = (a_n - \bar{a}_n) \otimes \mathbf{g} + \tilde{u}_n + \tilde{v}_n + \tilde{\kappa}_n \tag{4.4}$$

where $\{a_n\}$ is the transmitted data sequence, $\{\bar{a}_n\}$ is the detected sequence at normal VD output, $\mathbf{g} = [g_0, g_1, \cdots, g_{N_g-1}]$ is the GPR target response, and $\{\tilde{u}_n\}$, $\{\tilde{v}_n\}$ and $\{\tilde{\kappa}_n\}$ are the media noise, electronics noise and residual ISI, respectively, at normal VD input. When there is no bit error, $a_n - \bar{a}_n = 0$, otherwise, $(a_n - \bar{a}_n) \in \{+2, -2\}$. The possible error regions are those where $(a_n - \bar{a}_n) \in \{+2, -2\}$. We want to detect the occurrence of error events in the presence of media noise, electronics noise and residual ISI. However, if the normal VD makes some error at certain positions, *i.e.*, the normal VD fails to detect an error event, it is highly probable that the media noise, electronics noise and residual ISI overwhelm the signal $\{\bar{a}_n - a_n\} \otimes \mathbf{g}$. Thus, to be able to find out the possible bit error regions accurately, we need to filter out the distortions out of the signal $\{\bar{e}_n\}$, as much as possible, in the first place.

Figure 4.3 shows the estimated spectra of the three distortions for 5% jitter channel with SNR=36dB. In comparison, Figure 4.4 shows the estimated spectra of the four most dominant error events after passing through the GPR target.

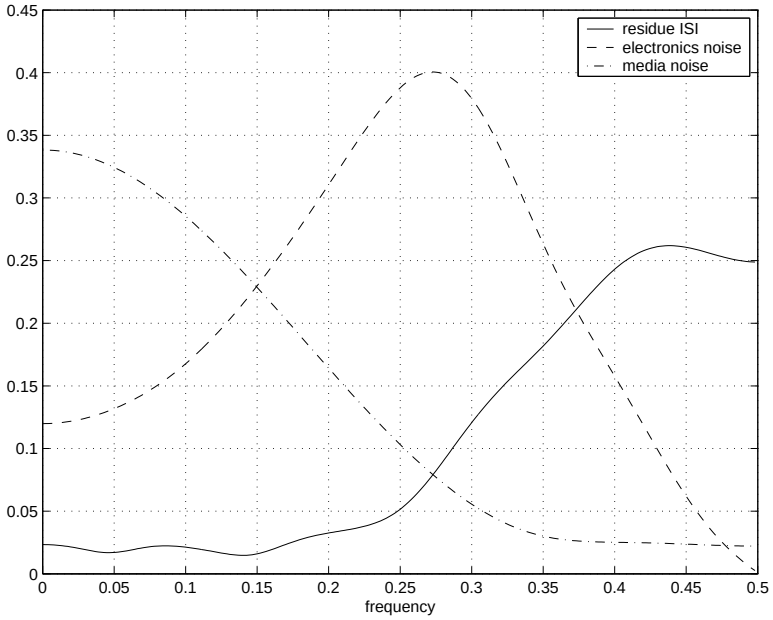

Figure 4.3: Spectra of residual ISI, electronics noise and media noise at normal VD input for 5% jitter channel and 36dB SNR.

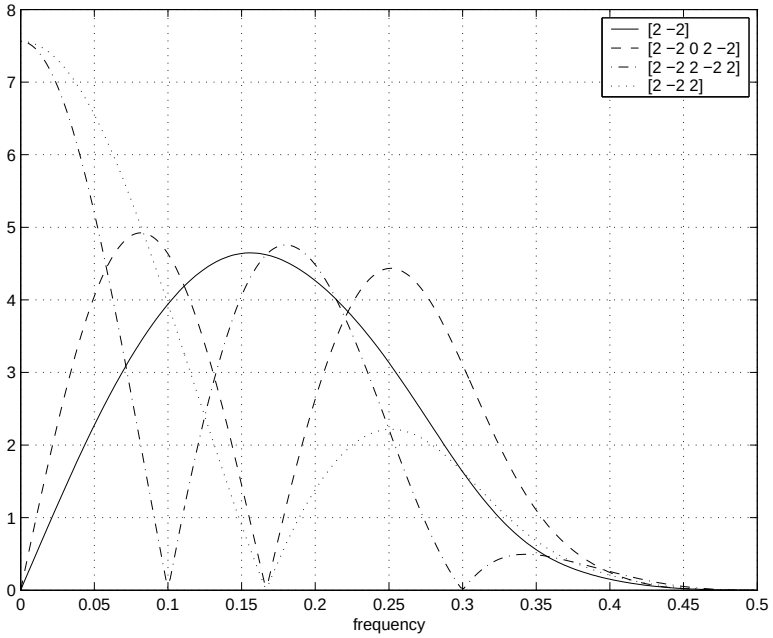

Figure 4.4: Spectrum of four most dominant error events passing through the target response channel.

Observe that the spectra of the dominant error events are quite different from those of the distortions in Figure 4.3. Therefore, an optimum filter to retrieve the energy of the error event present in $\{\bar{e}_n\}$ is a filter matched to the error event of interest.

Thus, the approach to identify the possible error regions is to pass the signal $\{\bar{e}_n\}$ through a bank of matched filters matched to the signal $(a_n - \bar{a}_n) \otimes \mathbf{g}$ caused by dominant error events, followed by a simple threshold detector on the outputs of matched filters to determine whether the bit position might be in error (see Figure 4.2).

For any possible bit error position, we may assume that the corresponding error region includes the bit positions around this bit with length L_p. This is the region over which re-detection will be done in the second-step of post-processing. Choosing suitable thresholds for each matched filter output defines the trade-off between performance gain and complexity. When the threshold is higher, the number of possible error regions is smaller thus reducing the complexity required for re-detection, while at the same time the number of undetected error regions will be larger thus limiting the possible gain in BER performance. Hence, practical thresholds should be chosen according to the channel under study. In practice, we can choose the thresholds according to

$$\gamma_{th} = \alpha_{th} e_o \tag{4.5}$$

where e_o is the maximum absolute value in the ideal output signal obtained by passing the signal $(a_n - \bar{a}_n) \otimes \mathbf{g}$ through the matched filter matched to itself, and the ratio $\alpha_{th} \in (0, 1)$ is chosen according to the output values of the matched filters due to real error events. Normally, we can set α_{th} to about 0.5. Whenever the absolute value of the output of any matched filter at instant n exceeds the corresponding threshold, the region around instant n with length L_p is identified

as a possible error region. In other words, the purpose of the matched filters is not to detect any particular error event that has occurred, instead, the purpose is to indicate the presence of a possible error.

4.3.2 Second Step: Re-detection of the Possible Bit Error Regions

After identifying all the possible error regions, the second step of the post-processing approach is to re-detect the bits in those regions using approaches, such as VD-MV and VD-NP, that incorporate the data-dependence of media noise.

First, we assume that the detected bits of normal VD outside any possible error region are reliable, and thus obtain the starting state and ending state of the trellis for each region. We also obtain the error signal $\bar{e}_n$ for the bit positions outside this region, which the predictors in VD-NP use for doing noise prediction.

Next, we re-detect the bits in the possible error regions using VD-MV or VD-NP approaches. We call these approaches as post-processor with mean and variance compensation for noise (PP-MV) and post-processor with data-dependent noise prediction (PP-NP), respectively. From Figure 4.1, we can observe that the VD-MV and VD-NP outperform the normal VD since they combat the data-dependence of media noise explicitly. We can expect PP-MV and PP-NP to achieve BER performances close to VD-MV and VD-NP at a fairly low cost of complexity increase since we only post-process the data in the post-processing regions and not the whole sequence.

Since the post-processors take data-dependent media noise characteristics into consideration during the detection of the bits in the identified possible error regions, the bit errors within these regions will be corrected within the ability of the post-processors, which in theory is upper-bounded by the performances of VD-MV and

VD-NP. However, in practice, the result of this post-processing approach is much more complicated. We might have right corrections of bit errors, which is good. On the other hand, we might also miss some real bit error positions during the first post-processing step. What is even worse is that we might even have some "false corrections" at the correct bit positions, *i.e.* the second post-processing step might result in increasing the bit errors for a given region than at normal VD output.

False correction happens because the bit error positions of VD-MV and VD-NP are different from those of the normal VD[2]. Thus, if a post-processing region corresponds to some bit error positions of VD-MV or VD-NP while not that of the normal VD, the re-detection of this regions may result in unwanted and wrong corrections. It is easy to see that this false correction problem will be more severe at low SNRs than high SNRs. At high SNRs, the bit error positions of VD-MV and VD-NP are mostly part of those of the normal VD. While at low SNRs, bit error positions of the three detectors are quite different, which makes the false correction problem to be quite severe. This problem can not be totally avoided by the post-processing approach, but can be mitigated by trying to identify the possible error regions accurately or using conservative criteria for correcting the bits. One approach is to use more matched filters to increase the accuracy in locating different error events while avoiding possible false correction regions. Another approach is to use two post-processors instead of one. Since the bit error positions of PP-MV and PP-NP at low SNRs are also quite different, if we use both of these post-processors (TWO-PP approach) for any post-processing region, we may choose to correct a bit only when both two post-processors agree on this. Of course, we may lose some performance in correcting the real bit errors in the TWO-PP approach, but the overall performance can still be improved since most of the false corrections can be avoided. At low SNRs, it was observed that the TWO-PP approach

[2]The 'bit error position' referred to in this statement means positions at which we would have seen errors if we had processed the complete sequence of equalizer output using these detectors, as done in Figure 4.1.

can outperform both PP-MV and PP-NP (see Figure 4.5). At high SNRs, the problem of false corrections becomes unimportant and the performance loss due to combining the outputs of two post-processors becomes the dominant effect of the TWO-PP approach. Hence, the TWO-PP approach is effective only at low SNRs.

4.3.3 Additional Comments

In this section, we provide some comments to distinguish the proposed post-processing approach presented above with existing parity-based post-processing (PPP) [38] and soft-output post-processing (SOPP) [42, 44] approaches.

It is a common practice now in magnetic recording systems to use parity check codes to help identify the occurrence and positions of the dominant error events and to correct them. Our approach is essentially different from PPP in that no redundant coding is needed to locate possible bit error positions. Hence code rate loss is avoided, and the resulting SNR gain can be used to enhance the recording density of a hard disk system. Also, different from PPP, the matched filters in our approach need to do only detection of the presence of an error and no classification of error is required.

Since our two-step post-processing approach is independent of any coding scheme, any parity check coding scheme can be still used along with our approach. That is, our approach can be also combined with parity check codes to provide more performance gains. Parity check codes can be used to determine whether there is a false correction in the post-processing regions, thus avoiding the false correction problems. Furthermore, since most of the dominant error events have been located and corrected in our post-processor, new parity check codes can be designed to focus on less dominant, mostly longer, error events. The new parity check codes shall have lower code rate loss, and combined with our post-processing approach, will provide protection against more error events. Thus, the BER performance can

be improved more significantly.

Our post-processing approach is also essentially different from the SOPP approach in [42, 44]. SOPP does data-dependent post-processing for each bit in the sequence, while our approach works only on a minor part (*e.g.* 0.77%, see the next section on simulation results) of the whole sequence. Thus, the complexity of our approach is much lower than that of SOPP. Note that it is hard to compare the BER performances of our approach with that of SOPP due to the differences in channel models and SNR definitions.

4.4 Analysis and Simulation Results

Recall that the motivation for the proposed two-step post-processing approach is to improve the BER performance of the normal VD at the cost of moderate increase of computational complexity, or to reduce the complexity of VD-MV and VD-NP by only processing a small portion of the whole sequence. In this section, we investigate the computational complexity and BER performance of the proposed post-processing approaches.

4.4.1 Computational Complexity

The additional computations in the two-step post-processing approach include passing the VD output sequence through the GPR target, obtaining and passing the error signal $\{\bar{e}_n\}$ through a set of matched filters, and re-detection of the bits in the post-processing regions.

Table 4.2 lists the computational complexities of the different post-processors, where N_g denotes the length of target response, L_m denotes the length of matched filters, N_m denotes the number of matched filters, N_p denotes the length of the

Table 4.2: Complexity of the proposed two-step post-processing approaches, in terms of the number of operations per branch metric.

	PP-MV	PP-NP	TWO-PP
$+/-$	$1+\frac{N_g+(L_m-1)\times N_m}{2^{N_g}}$ $+\alpha_p \times 3$	$1+\frac{N_g+(L_m-1)\times N_m}{2^{N_g}}$ $+\alpha_p \times (N_p+2)$	$1+\frac{N_g+(L_m-1)\times N_m}{2^{N_g}}$ $+\alpha_p \times (N_p+5)$
$\times$	$1+\frac{N_g-1+L_m\times N_m}{2^{N_g}}$ $+\alpha_p \times 2$	$1+\frac{N_g-1+L_m\times N_m}{2^{N_g}}$ $+\alpha_p \times (N_p+2)$	$1+\frac{N_g-1+L_m\times N_m}{2^{N_g}}$ $+\alpha_p \times (N_p+4)$

predictor, and α_p denotes the fraction of the overall sequence that is post-processed. Compare Table 4.2 with Table 4.1, we can see that the complexity increase due to post-processing is mainly determined by the number of matched filters, matched filter length and the post-processing ratio α_p. However, this also defines a trade-off here. If we want to reduce α_p, we need to use more matched filters with greater lengths.

4.4.2 BER Performance

The essential idea of our post-processing approach is to detect only a very small part of the whole sequence using the complicated approaches that account for the data-dependent media noise, while for most of the sequence, we only use a normal VD. Thus the BER performance of our post-processing approach is mainly determined by how well the real error regions are identified, whether the post-processors can correct the real bit errors and the number of false corrections. The BER after post-processing can be written as

$$\mathrm{BER}_{PP} = (1 + r_f - r_c) \cdot \mathrm{BER}_{VD} \tag{4.6}$$

where BER_{VD} denotes the BER of normal VD, r_f and r_c represent the ratios of false corrections and right corrections, respectively, over real bit errors.

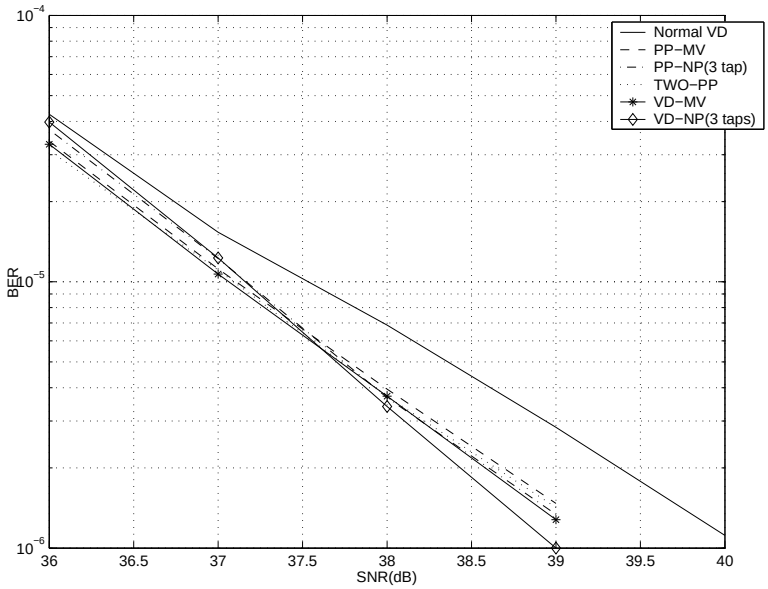

Figure 4.5: BER performances of the post-processing approaches.

4.4.3 Simulation Results

In this section, we show some simulation results of the post-processing approach under the following conditions: perpendicular magnetic recording channel with 5% jitter and linear density equal to 2.0, the 5-tap GPR targets and linear equalizers designed in Chapter 3 are used, 3-tap predictors are used for the PP-NP approach, four matched filters with length 7 matched to the four most dominant error events of normal VD, and the length of post-processors L_p is set to be 17.

Figure 4.5 shows the BER performances of the post-processing approach. The BER performances of the normal VD, VD-MV and VD-NP are also shown in Figure 4.5. At least 1000 error bits are collected for each estimate of BER.

It can be seen from Figure 4.5 that the BER performance of TWO-PP approach is the best at low SNRs (SNR=36dB), and it is even better than the performance of VD-MV and VD-NP. This is because the false correction problem is very serious at low SNRs and can be mostly avoided by the TWO-PP approach. At high SNRs (SNR>38dB), the false correction problem is not a serious problem. Hence, the

Table 4.3: Complexity of the post-processing approaches.

	$+/-$	$\times$
Normal VD	1	1
VD-MV	3	2
VD-NP	5	5
PP-MV	1.83	2.0177
PP-NP	1.85	2.0377
TWO-PP	1.87	2.0554

performance of TWO-PP approach is limited and the PP-NP approach performs best among all the post-processing approaches. It can be seen that the performance of the post-processing approach is upper-bounded by those of VD-MV and VD-NP, which is expected. We can also observe that the overall performances of the post-processing approaches are quite close to those of VD-MV and VD-NP. Thus, the performance gain over normal VD at a BER of 10^{-6} is about 1dB, while the performance loss compared to VD-MV and VD-NP is very small.

From the simulation results, we can also estimate the post-processing ratio

$$\alpha_p = \alpha_e \times L_p \tag{4.7}$$

where α_e is the ratio of total length of the post-processing regions over the input bit sequence length, and $L_p = 17$ is the length of each post-processing region. At SNR=39dB, we get (from simulations) $\alpha_e = 4.524 \times 10^{-4}$, and thus $\alpha_p = 4.524 \times 10^{-4} \times 17 = 0.77\%$, which means that only 0.77% of the detector input samples are being post-processed. Table 4.3 lists some numerical results of the complexities of different detection approaches.

From Table 4.3, we can see that the computational complexities of PP-MV and PP-NP are almost the same because the post-processing ratio α_p is very small. Even the complexity of TWO-PP is only slightly higher than PP-MV and PP-NP. It can be seen that the most complex operations, *i.e.*, division and logarithm, are

reduced by 99.23% in PP-MV and PP-NP compared to VD-NP and VD-MV. The number of additions is reduced by about 38.7% and 63.2% compared to VD-MV and VD-NP, respectively. Further, the number of mulplications is increased by about 100% and reduced by 49.5% compared to VD-MV and VD-NP, respectively. Since division and logarithm require much more actual computations than addition and multiplication, the overall complexity is reduced significantly.

In summary, the complexity of the proposed post-processing approach is much less than VD-MV and VD-NP at the cost of minor performance losses at high SNRs. At low SNRs, there is almost no performance loss and there might even be performance enhancement. In other words, we obtain a performance gain of 1dB over the normal VD at the cost of minor complexity increase.

4.5 Summary

In this chapter, we presented an overview of detection approaches that account for data-dependent media noise. Thereafter, we proposed a post-processing approach with three different post-processors. Computational complexities and BER performances of the two-step post-processing approach were investigated. We also present some computational and simulation results. It is shown that the post-processing approach can reduce the complexity of the complicated sequence detection approaches greatly with minor performance loss or even performance enhancement at certain SNRs.

Chapter 5

Analysis and Design of Sliding Block Viterbi Detector for Magnetic Recording Channels

Analysis of the performance and design of key parameters of sliding block Viterbi detector (SBVDet) for magnetic recording channels are presented in this chapter. We start with a short introduction of SBVDet approach. Thereafter, we present a detailed algorithm for doing error event analysis of VD with unknown starting and ending states. Through the error event analysis and simulation results, we show that SBVDet can increase the speed of VD without limit and with almost no influence on the BER performance and error event distribution. Finally, an intuitive approach to do error event analysis for simple PR targets is also presented.

5.1 Introduction

As introduced in Section 1.4.3, the SBVDet approach is quite an advantageous approach to enhance the detection speed. Our emphasis, in this chapter, is the performance analysis of the SBVDet approach on magnetic recording channels. This is motivated by the fact that the application of SBVDet to PR channels results in catastrophic and non-catastrophic error events due to the uncertainty

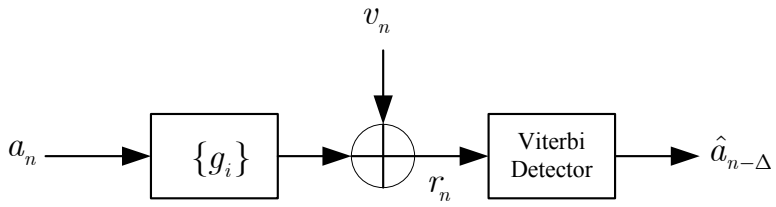

Figure 5.1: Model of partial response equalized recording channel with Viterbi detector.

associated with the starting and ending states in the trellis for each block. These events are in addition to the usual events that occur during conventional Viterbi detection for PR channels where the starting and ending states are known. In this chapter, through error event analysis, we not only throw light on the performance of SBVDet, but also provide guidelines for choosing the key parameters of the SBVDet structure.

We use the conventional hard disk drive systems to illustrate the performance of SBVDet. For the sake of convenience and without loss of generality, we assume in this chapter that the recording channel is perfectly equalized to a PR target and the channel noise at the Viterbi detector (VD) input is additive white Gaussian noise (AWGN). The resulting model of the recording channel, including the detector, is shown in Figure 5.1. Here, $\{a_n\}$ denotes the sequence of independent and identically distributed recorded bits, with each bit a_n being equally probable to be +1 or -1, and $\{v_n\}$ denotes the AWGN channel noise with power spectrum density $N_0/2$. Further, $\{g_i, i = 0, 1, \cdots, N_g\}$ denotes the bit response of the PR target, with $N_g + 1$ denoting the target length. Finally, $\{\hat{a}_{n-\Delta}\}$ denotes the detected bit sequence, with Δ being the delay with respect to the input a_n.

5.2 Sliding Block Viterbi Detector (SBVDet)

In conventional VD, the bit sequence is detected by processing the sequence of received samples in a serial manner, sample-after-sample, and the throughput rate is

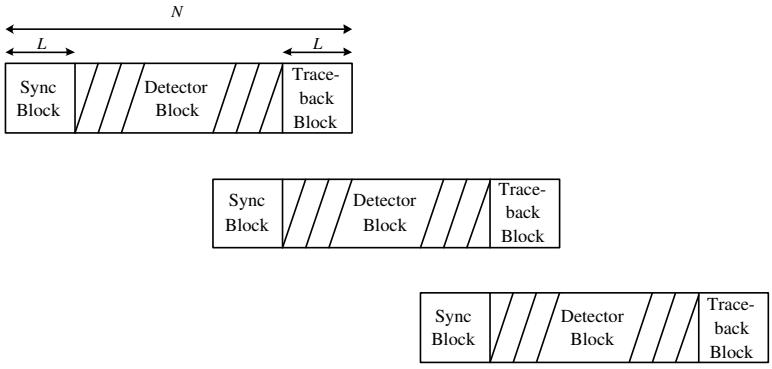

Figure 5.2: Sliding block Viterbi detection approach.

limited by the add-compare-select-unit (ACSU). To enhance the detection speed, we can use a sliding block detection approach as shown in Figure 5.2 [5]. The received sequence is divided into overlapping blocks of length N with the overlapping period being $2L$. The bits in each block are detected independently. The sync block and trace-back block of length L bits at the beginning and end, respectively, of each N-bit data block are used to provide the survivor path memory required to reliably detect the $N - 2L$ bits in the detector block.

Thus, using the sliding block detection approach, the detection speed can be enhanced according to the number of blocks used. Ideally, the speed can be enhanced infinitely by dividing the sequence into arbitrarily short blocks. However, as we show below, there exist some lower bounds for N and L to ensure reliable detection performance. The aim of the analysis that we present in this chapter is to develop a theoretical framework to help in the selection of appropriate values of N and L for the desired trade-off between complexity and performance. In fact, our analysis shows that the bounds on N and L are so low that they do not actually manifest as limitations to achieving practically meaningful high throughput implementations.

In SBVDet, since the starting and ending states of each block are unknown prior to detection, we meet with the problems of "synchronization errors" and "truncation errors", as stated in [53]. The *truncation errors* are caused by the

use of finite survivor depth L. The *synchronization errors* happen when we try to detect a sequence with all path metrics at an arbitrary instant before the current instant set to zero, although setting the metrics at an instant to zero is the best we can do when we do not have any information on the instants prior to this. It can be seen from analysis and simulations, as shown in the following sections, that the effect of these two errors tends to be negligible for bit positions far from the starting and ending positions. Therefore, by introducing an overlapping period of length $2L$ between two consecutive blocks, we can ensure that the whole sequence can be detected reliably if N and L are large enough. Note that the sync block and trace-back block in Figure 5.2 are used to handle the synchronization errors and truncation errors, respectively. Since the two kinds of errors are dual to each other, it's clear that we should choose the same length L for both sync block and trace-back block. Only the bits in detector blocks are viewed as detected bits.

5.3 Performance Analysis of SBVDet

In this section, we investigate the BER performance and error event distribution of SBVDet. It is desirable that the BER and error event distribution of SBVDet be close to that of conventional VD, *i.e.*, the detection speed is enhanced with almost no performance loss. The main part of this analysis is the development of a method to do error event characterization of SBVDet in the presence of synchronization and truncation errors. Of particular interest is to understand and expose the effect of catastrophic and non-catastrophic error events caused by these errors.

As stated in Section 5.2, in the SBVDet approach, we detect each block of bits independently without knowing the starting and ending states in the underlying trellis for each block. As a result, this gives rise to two problems: *truncation errors* and *synchronization errors*. These two errors are dual of each other. Therefore, we

will only consider synchronization errors here. The analysis of the effect of synchronization errors has been done [53] for decoding of convolutional codes which are not catastrophic[1]. But, for sequence detection on ISI channels such as in magnetic recording systems, we cannot use the conclusions in [53] directly. This is because the commonly used PR targets in magnetic recording result in "catastrophic error events" in the presence of synchronization errors. These error events are caused not by the noise but by the synchronization errors, and hence the SNR has no effect on the correct detection of the data patterns underlying such error events. Thus, we need to analyze the catastrophic error events to get the BER of SBVDet, which is different from the analysis in [53]. In addition to the catastrophic error events, the synchronization errors also cause non-catastrophic error events. Thus, to be able to investigate the BER performance of SBVDet, we need to consider the catastrophic and non-catastrophic error events caused by synchronization errors, in addition to the error events that are caused by noise.

5.3.1 Characterization of Catastrophic and Non-catastrophic Error Events

Altekar *et al.* [2] presented "error state diagram" based approaches for doing error event characterization of conventional VD for certain specific PR channels. In order to obtain error event characteristics of the SBVDet approach, we extend the algorithms in [2] in two ways. First, we present the error event characterization due to synchronization errors which to our knowledge has never been done by others. Secondly, our approach can be applied to any general PR target, while the approach in [2] is focused on standard PR targets of the form $G(D) = (1 - D)^m(1 + D)^n$, where D denotes 1-bit delay operator. Our approach consists of 3 steps and the

[1] A convolutional code is called catastrophic if a finite number of channel errors can cause an infinite number of decoded bit errors. Some methods have been proposed to avoid catastrophic codes [53].

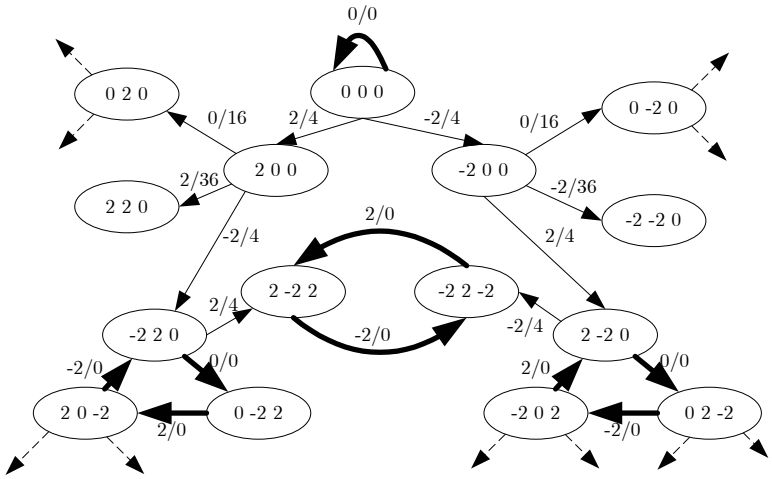

Figure 5.3: Part of the error state diagram for [1 2 2 1] channel.

details of these steps are given below. For the sake of convenience and without loss of generality, we take the widely used PR target for perpendicular magnetic recording $G(D) = 1 + 2D + 2D^2 + D^3$ (or, the channel with bit response $\mathbf{g}$=[1 2 2 1]) as an example for illustrating the principles underlying our 3-step approach.

A. Error State Diagram

As a first step to investigating the error event characteristics of SBVDet for a given PR target, we need to construct the underlying error state diagram. The error state diagram is a labeled directed graph $\mathcal{G}$. Input error sequences together with their corresponding squared output error sequences can be described as paths through this graph. Since the recorded bits belong to the binary alphabet $\mathcal{A} = \{-1, +1\}$, the corresponding alphabet for input error sequences will be $\mathcal{B} = \{-2, 0, +2\}$. Therefore, the number of states of the underlying error state diagram is 3^{N_g}, where N_g is the channel memory. Thus, there are $3^3 = 27$ states in the error state diagram for [1 2 2 1] channel and Figure 5.3 shows part of this. The edge label is given in the form $\mathcal{L}_{in}/\mathcal{L}_{out}$, where $\mathcal{L}_{in}$ and $\mathcal{L}_{out}$ denote the current input error symbol and the corresponding squared output error symbol, respectively. Note that it is for simplicity that we present only part of the error state diagram in Figure 5.3. It is

straightforward to obtain the complete error state diagram from Figure 5.3.

B. Searching for cycles in the error state diagram and catastrophic error events

In the presence of synchronization errors, some input error sequences may result in all-zero output. We call such error sequences as 'catastrophic error events' since it is impossible to detect the correct data underlying these error sequences irrespective of the noise level. It is clear that the spectrum of catastrophic error events must correspond to the spectral nulls of the channel response and also to cycles in the graph $\mathcal{G}$ where the $\mathcal{L}_{out}$ of each edge in the cycles is zero.

For the [1 2 2 1] channel, we have

$$1 + 2D + 2D^2 + D^3 = (1 + D)(1 + D + D^2), \tag{5.1}$$

resulting in spectrum nulls at $\omega_1 = \pi$, $\omega_2 = 2\pi/3$ and $\omega_3 = 4\pi/3$. Therefore, the spectrum of catastrophic error events associated with [1 2 2 1] channel can be written as

$$\begin{aligned} F_e(e^{jw}) &= \sum_n 2\pi a_0 \delta(w - \pi + 2n\pi) \\ &+ \sum_n 2\pi a_1 \delta(w - 2\pi/3 + 2n\pi) \\ &+ \sum_n 2\pi a_2 \delta(w - 4\pi/3 + 2n\pi) \end{aligned} \tag{5.2}$$

where $\delta(w)$ represents the Dirac delta function and the complex scalars a_0, a_1 and a_2 correspond to the strength of the spectral lines at frequencies π, $2\pi/3$ and $4\pi/3$, respectively. Consequently, the corresponding catastrophic error sequence can be

written as

$$e_n = a_0 e^{jn\pi} + a_1 e^{jn\frac{2\pi}{3}} + a_2 e^{jn\frac{4\pi}{3}}. \tag{5.3}$$

Ideally, we can obtain all possible catastrophic error sequences from (5.3) by determining all possible candidates for the triplet $\{a_0, a_1, a_2\}$ such that $e_n \in \{2, -2, 0\}$ for all n. Each $\{a_0, a_1, a_2\}$ gives rise to one such error event. Clearly, enumerating all possible $\{a_0, a_1, a_2\}$ in this way is very difficult. Therefore, we resort to the error state diagram and apply a search algorithm to obtain the catastrophic error sequences.

The search algorithm is as follows. Let $\mathcal{C}$ represent the set of cycles in the graph. Initialize $\mathcal{C}$ to empty set and an integer variable i to 1.

1. For each initial state s_i, search through the labels of all outbound edges. Initialize the path history $\mathcal{P}$ with s_i.
   (a) If every $\mathcal{L}_{out}$ is non-zero, then clear $\mathcal{P}$ and restart the searching algorithm from next initial state s_{i+1}.
   (b) Otherwise, if some $\mathcal{L}_{out}$ is zero for some edge and the edge connects s_i to state $s_{i,j}$, then append the path history $\mathcal{P}$ with $s_{i,j}$. Check whether $s_{i,j}$ has ever before appeared in $\mathcal{P}$.
      i. If $s_{i,j}$ has never before appeared in $\mathcal{P}$, then keep the path $\mathcal{P}$ and run the same search algorithm starting from $s_{i,j}$.
      ii. If $s_{i,j}$ has appeared before in $\mathcal{P}$, it means that a cycle is found from $s_{i,j}$ to $s_{i,j}$. Add this cycle as an entry in $\mathcal{C}$, clear $\mathcal{P}$ and restart the searching algorithm from next initial state s_{i+1}.
2. To do the search for cycles from the next initial state s_{i+1}, increment i by 1 and go to step (1) if $i \leq 3^{N_g}$.

Thus, the whole algorithm finishes when the search has been done for every initial

state s_i, $i = 1, 2, \cdots, 3^{N_g}$.

For the [1 2 2 1] channel, there are four cycles and are shown in Figure 5.3 using bold edges. The cycle associated with the all-zero state corresponds to correct detection output. The other three cycles correspond to catastrophic error events, which can not be eliminated by increasing SNR since the "Euclidean distances" associated with these events are zeros. Therefore, the catastrophic error events will result in "error-floor" effect in BER.

C. Searching for error fragments and non-catastrophic error events

There are also non-catastrophic error events due to synchronization/truncation errors. By analyzing these error events, we can arrive at guidelines for choosing sync/trace-back block length in the SBVDet approach, such that the effect of synchronization/truncation errors is negligible for the detection of bits in detector blocks.

We define error fragment as the error sequence which corresponds to some path in the graph $\mathcal{G}$ which starts from any state and ends in some cycle. Note that the definition here is different from that in [2], where the starting state and ending state of any error fragment must both be in some cycles. In order to search for all the error fragments, we use the modified depth-first search algorithm in [2] to obtain all the error fragments that may start from any state in the graph $\mathcal{G}$.

For illustration, Figure 5.4 lists all the error fragments with squared Euclidean distance less than 12 for [1 2 2 1] channel. A graph such as this is called "modified error state diagram" and we denote it by $\mathcal{H}$. The edges of this graph are labeled as $(\mathcal{L})/\mathcal{L}_{out}$ where $\mathcal{L}$ denotes the error fragment with $\mathcal{L}_{out}$ being the associated squared Euclidean distance. The states which form cycles are shown using "bold" state-group rings (compare Figure 5.3 with Figure 5.4).

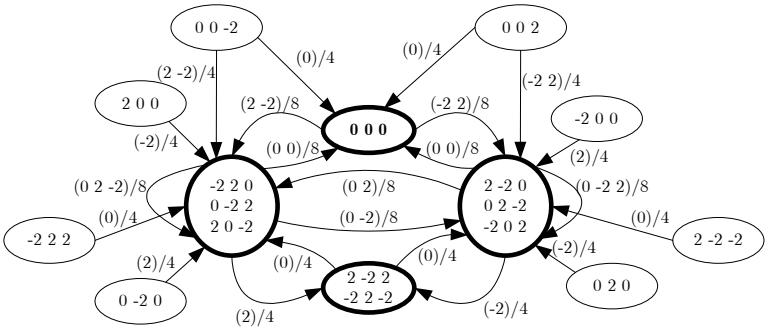

Figure 5.4: Modified error state diagram showing error fragments with squared Euclidean distance less than 12.

We may search for all the error events whose Euclidean distance is below some limit using the graph $\mathcal{H}$. All the error events end at some cycle in $\mathcal{G}$. Those error events that end at the all-zero state cycle are called 'closed error events', while other error events are called 'open error events'. We can run the depth-first search algorithm again on the modified error state diagram $\mathcal{H}$ to obtain all the open and closed error events with Euclidean distance below some limit. We may also obtain these error events by applying the depth-first search algorithm on the original graph $\mathcal{G}$, but its complexity is much higher than that of the above described 3-step approach.

5.3.2 Lower Bounds on N and L

We shall now outline the approach to arrive at the lower bounds on the block length N and sync/trace-back block length L. This is done by examining the extra error probability for each bit position within the block resulting from the catastrophic and non-catastrophic error events caused by the synchronization/truncation errors. Based on error event probabilities and distances, we can obtain BER union bound for each bit position due to these error events.

The error probability P_b for any particular bit position is bounded by the sum of the probabilities of the error events e which have an error at this particular bit

position (*i.e.*, the union bound). That is, we get

$$P_b \leq \sum_e \Pr(e) \tag{5.4}$$

where the probability of the error event, $\Pr(e)$, depends on the probabilities of the correct and incorrect data sequences ψ and $\hat{\psi}$, respectively, that make up e:

$$\Pr(e) = \Pr(\psi)\Pr(\hat{\psi} \mid \psi). \tag{5.5}$$

Since the channel noise is assumed to be AWGN, $\Pr(\hat{\psi} \mid \psi)$ can be given by [19]

$$\Pr(\hat{\psi} \mid \psi) \leq Q\left(\sqrt{d(\hat{\psi}, \psi)}/2\sigma\right) \tag{5.6}$$

where $d(\hat{\psi}, \psi)$ is the squared Euclidean distance associated with the error event corresponding to ψ and $\hat{\psi}$, $\sigma^2 = N_0/2$ is the noise variance (*i.e.*, with $T = 1$), and the $Q-$function is defined by

$$Q(x) = \frac{1}{\sqrt{2\pi}} \int_x^\infty e^{-t^2/2} \mathrm{d}t.$$

Clearly, the probabilities of the error events vary with the corresponding recorded sequences.

A. Catastrophic Error Events

We shall first consider the effect of catastrophic error events. It can be seen that every catastrophic error event imposes some constraint on the recorded bit sequence. For example, an input error symbol -2 can happen only when the corresponding recorded bit is 1. Thus, the number of recorded bit sequences that

may result in catastrophic error events is limited. Further, the probability of such sequences keeps decreasing exponential as the block length N increases.

We take the [1 2 2 1] channel as an example to illustrate the analysis. The catastrophic error event $\pm(+2,-2)^\infty$ (*i.e.* $\pm(+2,-2)$ repeated infinitely) happens only when the recorded bit sequence is $(1,-1)^\infty$ or $(-1,1)^\infty$. The error probability for each bit due to this event is 1/2 since the distance is 0. Assume that each recorded bit is independent and equally probable to be 1 or -1. Thus, we obtain the BER union bound due to this catastrophic error event for a block of length N as

$$2 \times (\frac{1}{2})^N \times \frac{1}{2}.$$

Similarly, we can obtain the BER union bound considering all the three catastrophic error events for [1 2 2 1] channel as

$$B_1 = \begin{cases} (\frac{1}{2})^N + (\frac{1}{2})^{2N/3-1} & \text{if } N = 3M \\ (\frac{1}{2})^N + (\frac{1}{2})^{(2N-5)/3} \cdot \frac{N-1}{3N} + (\frac{1}{2})^{(2N-2)/3} \cdot \frac{2N+1}{3N} & \text{if } N = 3M+1 \\ (\frac{1}{2})^N + (\frac{1}{2})^{(2N-1)/3} \cdot \frac{N+1}{3N} + (\frac{1}{2})^{(2N-4)/3} \cdot \frac{2N-1}{3N} & \text{if } N = 3M+2 \end{cases} \tag{5.7}$$

where $M = 0, 1, 2, \cdots$.

Figure 5.5 shows the BER union bound due to catastrophic error events for different block length N. Clearly, we should choose N large enough such that the BER due to catastrophic error events is negligible, for example $N > 30$ from Figure 5.5.

B. Non-catastrophic Error Events

Next, we shall consider the effect of non-catastrophic error events. The number of such error events is excessive, so we will not list them explicitly here. Instead, we

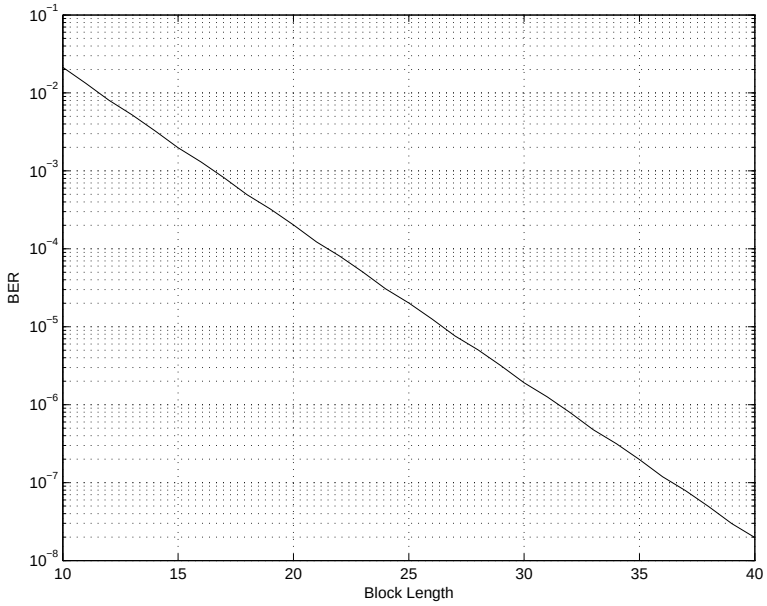

Figure 5.5: BER bound of SBVDet due to catastrophic error events.

focus on the union bound for bit error probabilities due to these error events and show some numerical results as follows.

Note that the error probabilities for different bit positions are different due to the error events caused by synchronization/truncation errors. Further, non-catastrophic error events may arise only for some particular recorded sequences. Thus, we need to examine all possible recorded sequences to compute the BER for each bit position.

We know that the non-catastrophic error events due to synchronization errors impose some constraints on the recorded sequences, the probability of which is roughly 2^{-n}, where n is the length of the error event. Thus, as n becomes large, the effect of synchronization errors also becomes negligible.

To give an example, we consider the case when SNR_1=14dB, where SNR_1 is defined as

$$\mathrm{SNR}_1(\mathrm{dB}) = 10\log_{10}\left(\frac{E_b}{N_0}\right) \tag{5.8}$$

where $E_b = \mathbf{g}^T\mathbf{g} = 10$ is the energy per bit. The BER for conventional VD without

synchronization/truncation errors is dominated by the error event with minimum squared distance 16:

$$P_{\text{b,conventional}} \approx Q\left(\frac{\sqrt{16}}{2\sigma}\right). \tag{5.9}$$

We can see that the non-catastrophic error events may have smallest squared distance equal to 4, and hence we can approximate the BER due to one of these error events as

$$P_e \approx \frac{1}{2^n} Q\left(\frac{1}{\sigma}\right) \tag{5.10}$$

where n is the length of the error event. Thus, at $\text{SNR}_1 = 14\text{dB}$ and $n = 30$, we can obtain that $P_e/P_{\text{b,conventional}} \approx 3.16 \times 10^{-6}$. That means the error events longer than 30 bits are negligible. Since the block length is likely to be greater than 30 (see Figure 5.5), all the open error events are negligible here. In summary, we only need to consider the closed error events whose length is less than 30.

In the above analyse, we only considered the error events due to synchronization errors. There are also closed error events due to AWGN electronics noise. In other words, the error events arising in conventional VD can also arise in SBVDet. For [1 2 2 1] channel, the most dominant error event in conventional VD is "$\pm(+2, -2)$", whose squared Euclidean distance is 16. The BER due to this error event is given by (5.9). We should also consider this error event when estimating the BER for each bit position. We can use (5.4) to obtain an estimate of the BER by considering the error events of length less than 30 caused by synchronization errors and AWGN (see (5.9)). Figure 5.6 shows the resulting BER for each bit positions for a block length of $N = 130$. Among the error events due to synchronization errors, we have considered only those with squared distance less than 12 since error events with smaller distances are most dominant. Observe from Figure 5.6 that the position-dependent BER has "transient" and "steady state" phases, and it goes from "transient phase" into "steady state phase" as the bit positions are further and further away from the start of a block. The BER at "steady state" is mainly

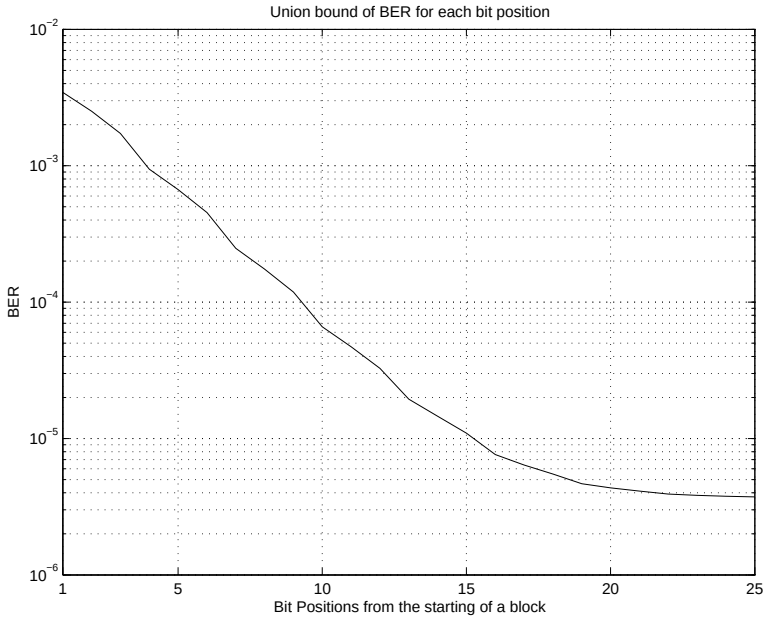

Figure 5.6: BER bound of SBVDet for each bit position arising from synchronization errors and AWGN at SNR_1=14dB.

determined by the dominant error event of conventional VD, while the effect of synchronization errors is negligible. Hence, by choosing an appropriate length L which is large enough, for example $L > 15$ from Figure 5.6, we may ensure that the bits in each detector block are detected as reliably as in conventional VD.

From the above analysis, we know that there exist some lower bounds for the block length N and the sync/trace-back block length L. These lower bounds are arrived at by imposing the requirement that the increase in BER in SBVDet, compared to conventional VD, caused by synchronization errors is within acceptable limits. When N and L are chosen according to this, the BER of the bits in each detector block would be quite close to that of the conventional VD. In other words, the BER performance of SBVDet would be almost the same as that of conventional VD (see Figure 5.7).

We can see that the lower-bounds on N and L are really small and they do not really act as serious hurdles pulling down the speed-enhancement capability of the SBVDet approach. We also remark that the lower-bound on the block-length N is

much smaller than that required in [28] to ensure satisfactory BER performance.

5.3.3 Additional Remarks

The method of analysis presented above is a general method that can be used in PRML systems with any GPR target. We would also like to remark that for some of the simple PR targets used in magnetic recording, we can do similar analysis of catastrophic/non-catastrophic error events intuitively without bothering to run the search algorithm through graphs. We present one such example in Section 5.6 where the PR target is $1 - D$.

Finally, we may add that some (if not all) of the catastrophic error events may be prevented by using appropriate code constraints and/or spectral-null constraints, non-symmetric PR targets, *etc.* Thus, we may have less stringent requirements on choosing N and L. To analyze such channels, the method presented in this chapter can still be used and we only need to modify the error state diagram accordingly.

In magnetic recording systems, it is now a common practice to use simple and efficient parity check codes in order to detect and/or correct the dominant error events at the VD output [43]. For example, even-parity or odd-parity check codes can be used to detect single bit errors in a block. Thus, it is also very important to examine the error event distribution for SBVDet. This will not be a problem intuitively, because the SBVDet is truly a ML detector and the effect of synchronization/truncation errors is negligible with reasonable choice of N and L. Thus, the error event distribution in SBVDet will be quite close to that of conventional VD (see Figure 5.8) and hence the overhead incurred in the use of parity check codes in SBVDet will be same as that in conventional VD.

5.4 Simulation Results

To demonstrate the performance of the SBVDet approach and the validity of our error event analysis, we use the perpendicular magnetic recording system model shown in Figure 5.1, which uses an ideal model of the PR equalized perpendicular recording channel. In our simulations, the PR target polynomial is chosen as $G(D) = 1 + 2D + 2D^2 + D^3$ [41]. The variance of AWGN channel noise is chosen according to the SNR_1 defined in (5.8).

The simulation was performed using data sequences of length 4000 bits each. Each sequence is divided into 40 blocks with the detector block length of each block being 100 bits (see Figure 5.2). From Figure 5.6, it can be seen that we may take the length of sync/trace-back blocks as $L = 15$. Thus, we have $N = 100+2L = 130$.

The overall BER performances of the conventional VD and SBVDet are shown in Figure 5.7. At least 1000 error bits are collected for every estimate of the BER. It can be seen that the BER performance of SBVDet is almost the same as that of conventional VD, thus verifying the analysis of Section 5.3. The corresponding error event distributions at SNR_1=14dB are shown in Figure 5.8. It can be seen that the error event distributions are also almost the same. The error event length in Figure 5.8 is defined as the length of the error sequence from the first error bit to the last error bit.

Thus, we may conclude from this simulation example and the analysis given earlier that SBVDet is able to increase the speed of VD with almost no loss in BER performance and no change in the error event distribution.

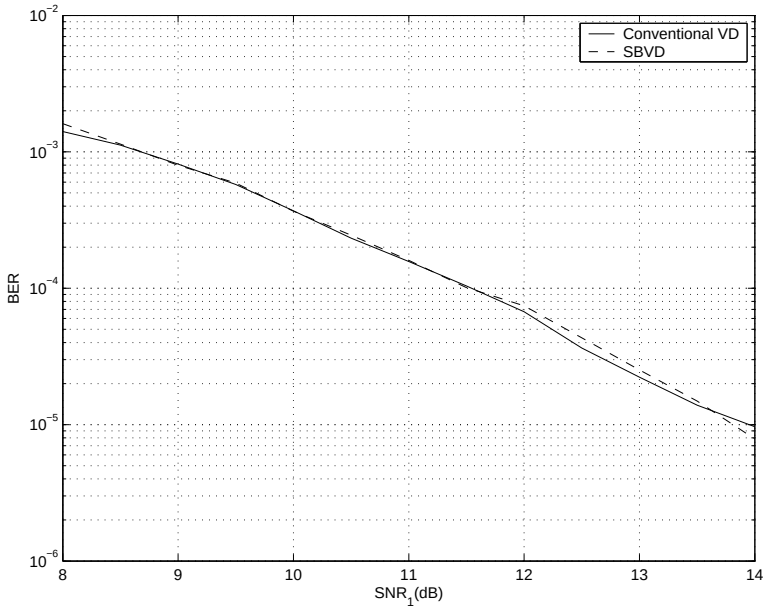

Figure 5.7: Comparison of BER performances of SBVDet and conventional VD.

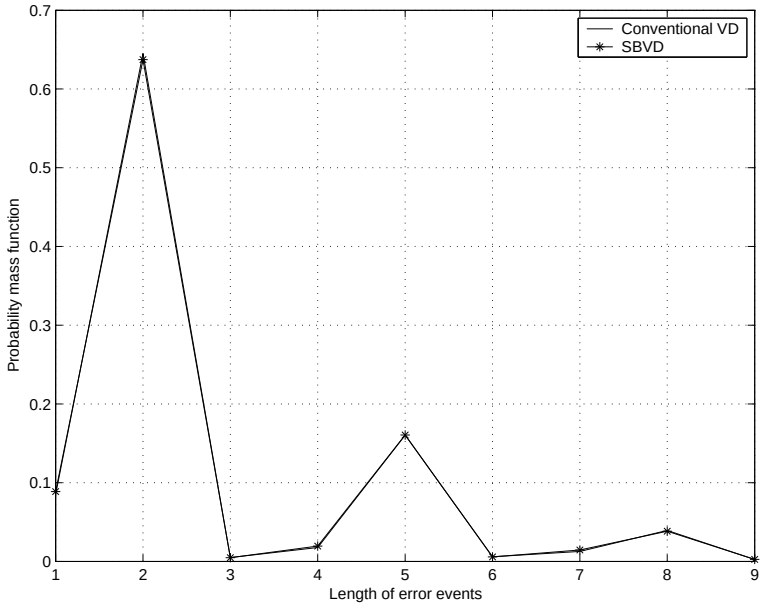

Figure 5.8: The error event distributions of SBVDet and conventional VD at SNR_1=14dB.

5.5 Conclusions

The SBVDet is an effective approach to enhance the speed of VD. To analyze the performance and design key parameters of SBVDet for magnetic recording systems, we have presented an algorithm for characterizing the error events of VD with unknown starting and ending states. Through numerical and simulation results, we have shown that the SBVDet approach can be used to overcome the speed bottleneck without influencing bit error probability and error event distribution if the block length and overlapping length are chosen properly.

5.6 Appendix: BER Analysis of VD with Unknown Starting and Ending States for $1-D$ channel

Recall from Section 5.3 that synchronization errors in SBVDet (*i.e.* inavailability of path metrics at the start of each block) cause additional error events (catastrophic and non-catastrophic), compared to conventional VD. A general search algorithm is presented in Section 5.3 for characterizing these events. In this Section, we show that for simple channels such as $1-D$, we may be able to characterize these events without going through the complications of constructing error state diagram and searching the resulting graph.

It can be easily seen that there is only one catastrophic error event for $1-D$ channel and is given by $\pm(2)^{\infty}$. This corresponds to the recorded bit sequences $+(1)^{\infty}$ and $-(1)^{\infty}$. Since the channel outputs for these two sequences are identical, the VD will not be able to discriminate between these two sequences. Further, this catastrophic error event cannot be eliminated by increasing the SNR.

With block length N (see Figure 5.2), let us assume that we transmit $\pm\{1, 1, \cdots, 1\}$

while detect it as $\pm\{-1,-1,\cdots,-1\}$. Then, (5.5) and (5.6) lead to $\Pr(\psi) = \frac{1}{2^N}$ and $\Pr(\hat{\psi} \mid \psi) = \frac{1}{2}$ since $d(\psi, \hat{\psi}) = 0$. Hence the resulting BER of each bit position due to this event is given by

$$\frac{1}{2^N} \times \frac{1}{2} \times 2 = \frac{1}{2^N}. \tag{5.11}$$

This means that the BER of every bit position is at least $\frac{1}{2^N}$ even if there is no noise at all. Thus, if the BER is required to be below 10^{-6}, we need to set the block length bigger than 20, which is a rough lower bound for the block length. In practice, we would choose a block length greater than this, since there are also other kinds of error events which will contribute to the bit error probabilities, as discussed below.

We shall now consider the case of the extra BER introduced by non-catastrophic error events caused by synchronization errors. The recorded and detected sequences corresponding to these events will have different starting states. The extra error events with length one and two are listed in Figure 5.9, for recorded sequences starting from the state "+1". The symmetric extension to the events starting from the state "-1" is straightforward. The solid line and dashed line represent the recorded and detected sequences, respectively, and the numbers above the lines are the outputs of the channel for the two possible sequences.

We can see that the first bit is wrong in the error events with length one and the first two bits are wrong in the error events with length two. The extra error probability of the first bit position introduced by error events with length one can

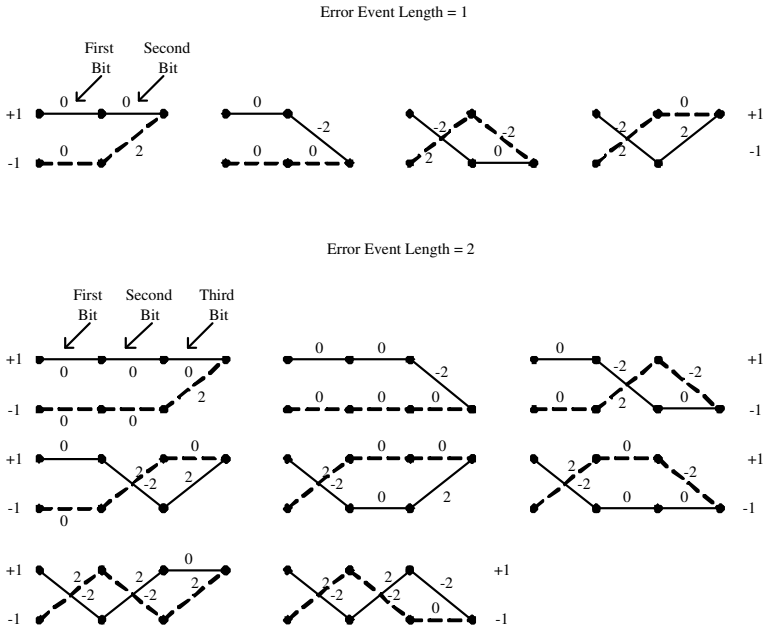

Figure 5.9: The non-catastrophic error events with length 1 and 2 for the $1-D$ channel caused by synchronization errors.

be obtained as

$$\begin{aligned} P_{1,1} &= \frac{1}{8} \times 4 \times Q\left(\frac{\sqrt{4}}{2\sigma}\right) + \frac{1}{8} \times 4 \times Q\left(\frac{\sqrt{20}}{2\sigma}\right) \\ &= \frac{1}{2}Q\left(\frac{1}{\sigma}\right) + \frac{1}{2}Q\left(\frac{\sqrt{5}}{\sigma}\right). \end{aligned} \tag{5.12}$$

Similarly, the extra error probabilities of the first and second bits introduced by error events with length two can be obtained as

$$P_{1,2} = P_{2,2} = \frac{1}{4}Q\left(\frac{1}{\sigma}\right) + \frac{1}{4}Q\left(\frac{3}{\sigma}\right) + \frac{1}{2}Q\left(\frac{\sqrt{5}}{\sigma}\right). \tag{5.13}$$

We can also get the extra error probabilities introduced by error events with length three, four and so on, similarly.

At high SNR, the probabilities $P_{1,1}$, $P_{1,2}$ and $P_{2,2}$ are dominated by the term with $Q(\frac{1}{\sigma})$. Considering only this dominant term, we get that the extra error

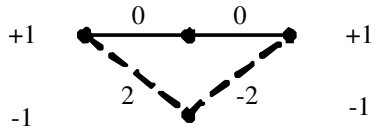

Figure 5.10: The dominant error event for $1-D$ channel in the absence of synchronization errors.

probabilities for the first and second bits as

$$P_1=\frac{1}{2}Q\left(\frac{1}{\sigma}\right)+\frac{1}{4}Q\left(\frac{1}{\sigma}\right)+\frac{1}{8}Q\left(\frac{1}{\sigma}\right)+\cdots=Q\left(\frac{1}{\sigma}\right)$$
$$P_2=\frac{1}{4}Q\left(\frac{1}{\sigma}\right)+\frac{1}{8}Q\left(\frac{1}{\sigma}\right)+\frac{1}{16}Q\left(\frac{1}{\sigma}\right)+\cdots=\frac{1}{2}Q\left(\frac{1}{\sigma}\right).$$

By inspection and induction, we get the extra error probability for the $(L+1)^{th}$ bit as

$$P_{L+1}=\left(\frac{1}{2}\right)^{L}Q\left(\frac{1}{\sigma}\right). \tag{5.14}$$

Thus, we see that the extra bit error probabilities of different bit positions are different and the bits nearer to the starting of the block suffer more. We can set the length of L (see Figure 5.2) to ensure that the extra bit error probabilities in detector blocks are negligible compared to the BER of the conventional VD. That is,

$$P_{L+1} \ll P_{b,conventional}.$$

For the $1-D$ channel, the BER of conventional VD is dominated by the error event with minimum distance as shown in Figure 5.10 and can be obtained as

$$P_{b,conventional} \approx Q\left(\frac{\sqrt{2}}{\sigma}\right). \tag{5.15}$$

From (5.14) and (5.15), we obtain

$$L \gg \log_2 \frac{Q(\frac{1}{\sigma})}{Q(\frac{\sqrt{2}}{\sigma})}. \tag{5.16}$$

Examples of the lower-bound on L given by (5.16) for $\mathrm{SNR}_1 = 12, 13$ and 14 dB are 12, 15 and 19, respectively.

Chapter 6

Conclusion and Future Work

In this thesis, we focused on signal detection approaches for high-density magnetic recording channels. There are some existing work on optimum signal detection techniques. However, the optimum approaches introduce high computational complexity and speed bottleneck. Therefore, we were motivated to explore the development of optimum or close-to-optimum signal processing approaches that have much lower complexity and/or break the speed bottleneck. In particular, we obtained optimum GPR targets for channels with jitter noise. Thereafter, we proposed a novel post-processing approach which can provide good trade-offs between BER performance and computational complexity. Finally, we presented the performance analysis and design of key parameters of sliding-block Viterbi detector to enhance the detection speed of magnetic recording.

In Chapter 1, we presented an overview of magnetic recording systems including characteristics of channel distortions, and briefly surveyed the existing techniques on related topics. Our motivation of research was also presented in Chapter 1.

Chapter 2 presented background knowledge on signal processing techniques for magnetic recording channels. We introduced the discrete-time channel models and

the basic principles of equalization and detection in this chapter.

Optimum joint PR target and equalizer design for high-density magnetic recording channel with jitter noise was presented in Chapter 3. A new cost function, which accounts for the data-dependent nature of jitter noise, was developed based on minimum mean square error criterion. Using the step response based channel model, we derived expressions for the statistics required to compute the optimum equalizer and target in the presence of jitter noise. We also derived a bit response based model for the jitter noise channel. We presented an approach for doing simulations as well as analytical computations for the jitter noise channel, without resorting to the widely used Taylor series approximations. We presented computational and simulation results to show that while the targets designed without accounting for the jitter lead to error-floor in the bit error rate (BER) performance, the targets designed by our approach give significant performance improvement under high jitter conditions, with no sign of error-floor effect for the range of signal to noise ratios considered.

A novel two-step post-processing approach for signal detection in magnetic recording channels with jitter noise was proposed in Chapter 4. The first step is to identify all the possible error regions from the normal Viterbi detector (VD) output using a simple threshold-based approach, and the second step is to re-detect only these regions using approaches that account for the data-dependent characteristics of jitter noise. We presented numerical and simulation results which show that the proposed post-processing approach can improve the BER performances of traditional VD approach significantly with minor increase in computational complexity.

Sliding block Viterbi detection (SBVDet) approach is an effective approach that can enhance the detection speed. We presented the performance analysis and design of key parameters of the sliding block detection approach for magnetic recording channels in Chapter 5. We presented a detailed algorithm for doing error

event analysis of VD with unknown starting and ending states. Through the error event analysis and simulation results, we showed that SBVDet can increase the speed of VD without limit and with almost no influence on the BER performance and error event distribution. We also presented an intuitive approach to do error event analysis for simple PR targets.

Future Work

There are some issues that remain to be solved in the signal detection approaches that are presented in this thesis for high-density magnetic recording channels with jitter noise.

1. The MMSE criterion used in this thesis when designing the optimum PR targets and equalizers is based on the assumption that each transmitted sequence is equally probable. The data-dependence of jitter noise is accounted for in an implicit way. We may modify the MMSE criterion, for example adding more weight on the data patterns that might result in higher jitter noise, to provide better suppression of jitter noise when designing the targets and equalizers.

2. The post-processors used in our two-step post-processing approach are based on estimated characteristics of media noise. This estimation approach assumed the media noise to be additive on the useful signal. We are not using the accurate channel model based on transition jitter to estimate the jitter noise samples. Thus, theoretical/numerical work can be done to develop better post-processors that account for transition jitter directly instead of additive jitter noise.

3. Although Viterbi algorithm is still widely used in magnetic recording sys-

tems, optimum MAP algorithms, such as the BCJR algorithm, will soon start to be used in practical magnetic recording systems due to the fast development of VLSI techniques. Thus, practical approaches, especially low-complexity/high-speed implementations of those complicated and recursive algorithms will have higher practical values.

We believe that the issues listed above will extend our work to provide better performances and higher practical values for emerging magnetic recording systems.

Bibliography

[1] (2005) Hitachi achieves industry-leading areal densities via perpendicular recording. [Online]. Available: http://www.hitachigst.com/hdd/research/recording_head/pr/

[2] S. A. Altekar, M. Berggren, B. E. Moision, P. H. Siegel, and J. K. Wolf, "Error-event characterization on partial-response channels," *IEEE Trans. Inform. Theory*, vol. 45, no. 1, pp. 241–247, Jan. 1999.

[3] J. W. M. Bergmans, *Digital Baseband Transmission and Recording.* Kluwer Academic Publishers, 1996, ch. 6.

[4] P. J. Black and T. H. Meng, "A 140-Mb/s, 32-state, radix-4 Viterbi decoder," *IEEE J. Solid-State Circuits*, vol. 27, no. 12, pp. 1877–1885, Dec. 1992.

[5] ——, "A 1-Gb/s, four-state, sliding block Viterbi decoder," *IEEE J. Solid-State Circuits*, vol. 32, no. 6, pp. 797–805, Jun. 1997.

[6] B. Brickner and J. Moon, "Combating partial erasure and transition jitter in magnetic recording," *IEEE Trans. Magn.*, vol. 36, no. 2, pp. 532–536, Mar. 2000.

[7] J. Caroselli, S. A. Altekar, P. McEwen, and J. K. Wolf, "Improved detection for magnetic recording systems with media noise," *IEEE Trans. Magn.*, vol. 33, no. 5, pp. 2779–2781, Sep. 1997.

[8] J. Caroselli and J. K. Wolf, "Application of a new simulation model for media noise limited magnetic recording channels," *IEEE Trans. Magn.*, vol. 32, no. 5, pp. 3917–3919, Sep. 1996.

[9] L. Chen, *Investigation on target design for perpendicular magnetic recording channels.* M.Eng Thesis, Dept. of Electrical & Computer Eng., National University of Singapore, 2004.

[10] M. Chen and E. A. Trachtenberg, "Detection for channels with transition noise," *IEEE Trans. Magn.*, vol. 34, no. 3, pp. 750–753, May 1998.

[11] R. D. Cideciyan, F. Dolivo, R. Hermann, W. Hirt, and W. Schott, "A PRML system for digital magnetic recording," *IEEE J. Select. Areas Commun.*, vol. 10, no. 1, pp. 38–56, Jan. 1992.

[12] J. D. Coker, E. Eleftheriou, R. L. Galbraith, and W. Hirt, "Noise-predictive maximum likelihood (NPML) detection," *IEEE Trans. Magn.*, vol. 34, no. 1, pp. 110–117, Jan. 1998.

[13] T. Conway, "Implementation of high speed Viterbi detectors," *Electronics Letters*, vol. 35, no. 24, pp. 2089–2090, Nov. 1999.

[14] G. Fettweis, H. Dawid, and H. Meyr, "Minimized method Viterbi decoding: 600 Mbit/s per chip," in *Proc. IEEE Intl. Conf. Global Telecommun. (GLOBECOM)*, San Diego, CA, Dec. 1990, pp. 1712–1716.

[15] G. Fettweis and H. Meyr, "Parallel Viterbi algorithm implementation: Breaking the ACS-bottleneck," *IEEE Trans. Commun.*, vol. 37, pp. 785–790, Aug. 1989.

[16] ——, "A 100 Mbit/s Viterbi decoder chip: Novel architecture and its realization," in *Proc. IEEE Intl. Conf. Commun. (ICC)*, Atlanta, GA, Apr. 1990, pp. 463–467.

[17] ——, "High-rate Viterbi processor: A systolic array solution," *IEEE J. Select. Areas Commun.*, vol. 8, pp. 1520–1534, Oct. 1990.

[18] ——, "High-speed parallel Viterbi decoding: Algorithm and VLSI-architecture," *IEEE Commun. Mag.*, pp. 46–55, May 1991.

[19] G. D. Forney, "Maximum-likelihood sequence estimation of digital sequences in the presence of intersymbol interference," *IEEE Trans. Inform. Theory*, vol. 18, pp. 363–378, May 1972.

[20] R. D. Gitlin and S. B. Weinstein, "Fractionally-spaced equalization: An improved digital transversal equalizer," *Bell Syst. Tech. J.*, vol. 60, pp. 275–296, Feb. 1981.

[21] S. Iwasaki, "Discoveries that guided the beginning of perpendicular magnetic recording," *J. Magn. Magn. Mater.*, vol. 235, pp. 227–234, Oct. 2001.

[22] S. Iwasaki and Y. Nakamura, "An analysis for the magnetization mode for high density magnetic recording," *IEEE Trans. Magn.*, vol. 13, no. 5, pp. 1272–1277, Sep. 1977.

[23] A. Kavcic and J. M. F. Moura, "The Viterbi algorithm and Markov noise memory," *IEEE Trans. Inform. Theory*, vol. 46, no. 1, pp. 291–301, Jan. 2000.

[24] A. Kavcic and A. Patapoutian, "A signal-dependent autoregressive channel model," *IEEE Trans. Magn.*, vol. 35, no. 5, pp. 2316–2318, Sep. 1999.

[25] P. Kovintavewat, I. Ozgunes, E. M. Kurtas, J. R. Barry, and S. W. McLaughlin, "Generalized partial response targets for perpendicular recording with jitter noise," *IEEE Trans. Magn.*, vol. 38, no. 5, pp. 2340–2342, Sep. 2002.

[26] I. Lee and J. L. Sonntag, "A new architecture for the fast Viterbi algorithm," *IEEE Trans. Commun.*, vol. 51, no. 10, pp. 1624–1628, Oct. 2003.

[27] L. Li, *Equalization and detection for perpendicular channels with media noise.* B.Eng Thesis, Dept. of Electrical & Computer Eng., National University of Singapore, 2004.

[28] H. D. Lin and D. G. Messerschmitt, "Algorithms and architectures for concurrent Viterbi decoding," in *Proc. IEEE Intl. Conf. Commun. (ICC)*, Boston, MA, Jun. 1989, pp. 836–840.

[29] H. Melbye and C. Chi, "Nonlinearities in high density digital recording," *IEEE Trans. Magn.*, vol. 15, no. 5, pp. 746–748, Sep. 1978.

[30] J. Moon, "Discrete-time modeling of transition-noise-dominant channels and study of detection performance," *IEEE Trans. Magn.*, vol. 27, no. 6, pp. 4573–4578, Nov. 1991.

[31] ——, "The role of SP in data-storage," *IEEE Signal Processing Mag.*, vol. 15, no. 4, pp. 54–72, Jun. 1998.

[32] ——, "Signal-to-noise ratio definition for magnetic recording channles with transition noise," *IEEE Trans. Magn.*, vol. 36, no. 5, pp. 3881–3883, Sep. 2000.

[33] J. Moon and L. R. Carley, "Performance comparison of detection methods in magnetic recording," *IEEE Trans. Magn.*, vol. 26, no. 6, pp. 3155–5172, Nov. 1990.

[34] J. Moon and J. Park, "Pattern-dependent noise prediction in signal-dependent noise," *IEEE J. Select. Areas Commun.*, vol. 19, no. 4, pp. 730–743, Apr. 2001.

[35] J. Moon and W. Zeng, "Equalization for maximum likelihood detectors," *IEEE Trans. Magn.*, vol. 31, no. 2, pp. 1083–1088, Mar. 1995.

[36] Y. Nishida, H. Sawaguchi, A. Kuroda, H. Takano, H. Aoi, and Y. Nakamura, "Noise characteristics of double-layered perpendicular media," *J. Magn. Magn. Mater*, vol. 235, pp. 454–458, Oct. 2001.

[37] T. Oenning and J. Moon, "Modeling the Lorentzian magnetic recording channel with transition noise," *IEEE Trans. Magn.*, vol. 37, no. 1, pp. 583–591, Jan. 2001.

[38] Y. Okamoto, S. Funano, H. Osawa, H. Saito, H. Muraoka, and Y. Nakamura, "A study on post-processing for PRML system with AR channel model in perpendicular magnetic recording," in *Proc. IEEE Intl. Magn. Conf. (INTERMAG)*, Boston, MA, Mar. 2003, pp. DT–18.

[39] Y. Okamoto, N. Masunari, H. Yamamoto, H. Osawa, H. Saito, H. Muraoka, and Y. Nakamura, "Jitter-like noise cancellation using AR model of PR channel in perpendicular magnetic recording," *IEEE Trans. Magn.*, vol. 38, no. 5, pp. 2349–2351, Sep. 2002.

[40] Y. Okamoto, H. Osawa, H. Saito, H. Muraoka, and Y. Nakamura, "Performance of PRML systems in perpendicular magnetic recording channel with jitter-like noise," *J. Magn. Magn. Mater*, vol. 235, pp. 259–264, Oct. 2001.

[41] Y. Okamoto, H. Sumiyoshi, T. Kishigami, M. Akamatsu, H. Osawa, H. Saito, H. Muraoka, and Y. Nakamura, "A study of PRML systems for perpendicular recording using double layered medium," *IEEE Trans. Magn.*, vol. 36, no. 5, pp. 2164–2166, Sep. 2000.

[42] H. Sawaguchi, M. Izumita, and S. Mita, "Soft-output post-processing detection for prml channels in the presence of data-dependent media noise," in *Proc. IEEE Intl. Conf. Global Telecommun. (GLOBECOM)*, San Francisco, CA, Dec. 2003, pp. 3913–3920.

[43] H. Sawaguchi, S. Mita, and J. K. Wolf, "A concatenated coding technique for partial response channels," *IEEE Trans. Magn.*, vol. 37, no. 2, pp. 695–703, Mar. 2001.

[44] H. Sawaguchi, Y. Nashida, and T. Nakagawa, "Performance analysis of soft-ouput post-processing detection for data-dependent media noise channels," *IEEE Trans. Magn.*, vol. 40, no. 4, pp. 3108–3110, Jul. 2004.

[45] H. Sawaguchi, Y. Nishada, H. Takano, and H. Aoi, "Performance analysis of modified PRML channels for perpendicular recording systems," *J. Magn. Magn. Mater*, vol. 235, pp. 265–272, Oct. 2001.

[46] H. Sun, G. Mathew, and B. Farhang-Boroujeny, "Detection techniques for high-density magnetic recording," *IEEE Trans. Magn.*, vol. 41, no. 3, pp. 1193–1199, Mar. 2005.

[47] A. Taratorin, D. Cheng, and E. Marinero, "Media noise, nonlinear distortions and thermal stability in high-density recording," *IEEE Trans. Magn.*, vol. 36, no. 1, pp. 80–85, Jan. 2000.

[48] G. J. Tarnopolsky, "Hard disk drive capacity at high magnetic areal density," *IEEE Trans. Magn.*, vol. 40, no. 1, pp. 301–306, Jan. 2004.

[49] H. Thapar and A. M. Patel, "A class of partial response systems for increasing storage density in magnetic recording," *IEEE Trans. Magn.*, vol. 23, no. 5, pp. 3666–3668, Sep. 1987.

[50] H. K. Thapar and J. M. Cioffi, "A block processing method for designing high-speed Viterbi detectors," in *Proc. IEEE Intl. Conf. Commun. (ICC)*, Boston, MA, Jun. 1989, pp. 1096–1100.

[51] K.-H. Tzou and J. G. Dunham, "Sliding block decoding of convolutional codes," *IEEE Trans. Commun.*, vol. 29, no. 9, pp. 1401–1403, Sep. 1981.

[52] A. J. Viterbi, "Error bounds for convolutional codes and an asymptotically optimum decoding algorithm," *IEEE Trans. Inform. Theory*, vol. 13, pp. 260–269, Apr. 1967.

[53] A. J. Viterbi and A. J. Omura, *Principles of Digital Communication and Coding*. McGraw-Hill, 1979, ch. 4,5.

[54] D. Weller and A. Moser, "Thermal effect limits in ultrahigh-density magnetic recording," *IEEE Trans. Magn.*, vol. 35, no. 6, pp. 4423–4439, Nov. 1999.

[55] R. Wood, Y. Sonabe, Z. Jin, and B. Wilson, "Perpendicular recording: The promise and the problems," *J. Magn. Magn. Mater.*, vol. 235, pp. 1–9, Oct. 2001.

[56] H. Yang and G. Mathew, "Joint design of optimum PR target and equalizer for recording channels with jitter noise," *IEEE Trans. Magn.*, vol. 42, no. 1, pp. 70–77, Jan. 2006.

[57] N. M. Zayed and L. R. Carley, "Equalization and detection for nonlinear recording channels with correlated noise," *IEEE Trans. Magn.*, vol. 35, no. 5, pp. 2295–2297, Sep. 1999.

[58] W. Zeng and J. Moon, "Modified Viterbi algorithm for a jitter-dominant $1 - D^2$ channel," *IEEE Trans. Magn.*, vol. 28, no. 5, pp. 2895–2897, Sep. 1992.

List of Publications

1. Hongming Yang and George Mathew, "Joint design of optimum PR target and equalizer for recording channels with jitter noise," *IEEE Trans. Magn.,* vol. 42, no. 1, pp. 70-77, Jan. 2006.

2. Hongming Yang and George Mathew, "A novel post-processing approach for signal detection in recording channels with jitter noise" *To be submitted to IEEE Transactions on Magnetics (Under preparation).*